Elucidating the structure and improving the cellular uptake of HexM, a candidate for enzyme replacement therapy of GM2 gangliosidosis

by

Graeme Benzie

A Thesis submitted to the Faculty of Graduate Studies of
The University of Manitoba
in partial fulfillment of the requirements for the degree of

MASTER OF SCIENCE

Department of Microbiology
University of Manitoba
Winnipeg

Abstract

Tay-Sachs disease and Sandhoff disease are genetic disorders resulting from mutations in genes *HEXA* or *HEXB*, which code for the α- and β-subunits of the heterodimer β-hexosaminidase A (HexA), respectively. HexA is a lysosomal glycosidase responsible for degrading GM2 ganglioside (GM2), a glycolipid found in the plasma membrane of neurons. Loss of HexA causes GM2 accumulation in neurons and deterioration of motor and cerebral function, typically resulting in death by age 4. Previously, the critical features of the α- and β-subunits of HexA were combined into a single engineered subunit (μ) to create a stable homodimeric version of HexA, known as HexM. HexM is twice as active as HexA, degrades GM2 both *in cellulo* and *in vivo*. Two major issues that often impede ERT development include the inability to produce therapeutic enzyme in sufficient quantities and inadequate enzyme phosphorylation, which is necessary for uptake into lysosomes of affected cells by the manose-6-phophate pathway. Here I demonstrate that HexM can be produced in gram-scale quantities, making it a promising candidate for enzyme replacement therapy (ERT) and that lysosomal uptake of HexM via the mannose-6-phosphate receptor can be enhanced (3- to 4- fold) by co-expressing HexM with an engineered Glc-NAc-1-phosphotransferase that hyper-phosphorylates lysosomal proteins. I also produced a HexM mutant incapable of hydrolyzing substrate and investigated methods of binding HexM to GM2AP to form a long-lived complex capable of being assessed by either transmission electron microscopy or x-ray crystallography. A crystal structure of HexM, combined with mass spectrometry-based glycoform analysis also revealed that HexM retains a fold and glycosylation pattern consistent with HexA. My studies further advance HexM as a potential ERT for Tay-Sachs disease and Sandhoff disease

Acknowledgments

I would like to express my sincerest gratitude to my supervisor Dr. Brian Mark, for his continuous support of my studies and research. His knowledge and guidance helped immensely me throughout my research and in writing this thesis.

I would also like to thank my committee members: Dr. Barbara-Triggs Raine and Dr. Peter Pelka for their encouragement and insightful comments during meetings.

I greatly appreciated being a part of the Mark lab, all my lab mates were helpful and always willing to provide support or discuss approaches to research. I would like to thank Vincent Jung for his knowledge and support in maintaining eukaryotic cell lines

I would like to thank my mother, whose love and support provided me with the education and mental fortitude to overcome life's difficult challenges.

Finally, I would like to acknowledge the following people and organizations for their contributions to my research:

Dr. Don Mahuran for providing the *HEK293TABKO-HexM-His* cell line which was fundamental to purifying HexM for analysis.

Dr. Stuart Kornfeld for providing *pcDNA6/V5-His-GlcNAc-1-PT* plasmid for the HexM phosphorylation analysis and cellular uptake assays.

Dr. Rick Hemming for his guidance and assistance culturing Tay-Sachs Disease fibroblast cells for the HexM cellular uptake assays.

Dr. Gil Privé for providing the *HEK293T-GM2AP-Protein A* cell line which was used to purify GM2AP for HexM pulldown assays.

Dr. Timothy Booth for providing access to his transmission electron microscope for imaging HexM.

Daniel Beniac and Shannon Heibert for their technical assistance with the FEI Tecnai F20 transmission electron microscope and processing the images of HexM

Dr. Helene Perrault for providing mass spectrometry data analysis with the assistance of Taylor Battelino and Tyler Tran

TABLE OF CONTENTS

Abstract 2
Acknowledgments 3
Table of Contents 4
List of Tables 6
List of Figures 7
Abbreviations 9

1. Introduction 11
1.0 Lysosomal Storage Disorders 11
1.1 GM2 gangliosidoses 11
1.2 Hex Isozymes 12
1.3 Synthesis and Transportation of HexA 13
1.4 The Role of GM2AP and HexA in the Lysosome 15
1.5 Genetic Screening for GM2 Gangliosidosis 15
1.6 Animal Models for GM2 gangliosidoses 16
1.7 Experimental GM2 Gangliosidosis Therapies 16
1.7.1 Pharmacological Chaperone Therapy 17
1.7.2 Substrate Reduction Therapy 19
1.7.3 Enzyme Replacement Therapy 19
1.7.4 Creation of HexM 20
1.8 Thesis Objectives 24

2. Materials and Methods 24
2.0 Plasmid 24
2.1 Cell Cultures 25
2.1.1 Cell Media 26
2.1.2 Bacterial Strains 27
2.1.3 Culture Media 27
2.2 Production of HexM 28
2.2.1 HexM Activity Assay 28
2.2.2 Long-term Stability Assay 29
2.3 Histidine Tag Removal from a N-acetylglucosamine-1-phosphotransferase plasmid 30
2.4 HexM Phosphorylation Analysis 31
2.4.1 Cellular Uptake assay using immortalized Tay-Sachs Disease (TSD) Fibroblasts 32
2.5 Mass Spectroscopy Analysis 32
2.6 Transmission Electron Microscopy Imaging 33
2.7 Production of HexM Crystals and X-ray Crystallographic Structure 33
2.8 Production of HexME322Q (loss of function mutant) 34
2.8.1 HexME322Q HexABKOHEK293T Cell Transfection 38
2.9 Production of GM2AP 38
2.10 Production of Intraendolysosomal-like Liposomes 39
2.9.1 Dynamic Light Scattering Analysis 40
2.10 HexM-GM2AP Pulldown Assay 40

3. Results and Discussion 41

3.1.0 Production and biochemical analysis of HexM 41
3.1.1 Increasing the production of HexM 41
3.1.2 MUGS Activity Assay 45
3.1.3 Long Term Stability Experiment 47
3.2.0 Enhancing the cellular uptake of HexM 48
3.2.1 Production of GlcNAc-1-PT-NoHis 50
3.2.2 Co-Transfection of HexM and GlcNAc-1-PT-NoHis 52
3.2.3 Cellular Uptake assay comparing PhosHexM and HexM 53
3.2.3 Mass Spectrometry Glycoform Analysis 56
3.3.0 Structural Studies of HexM 58
3.3.1 X-ray crystallographic structural analysis of HexM 58
3.3.2 HexM active site 60
3.3.3 Structural analysis of HexM β-subunit interface 61
3.3.4 Orientation of HexM monomers 62
3.4.0 Complexing HexM with GM2AP to gain insight into GM2 turnover 63
3.4.1 HexME322Q activity assessment 63
3.4.2 TEM Negative Stain Imaging 69
3.4.3 Production of GM2AP 72
3.4.4 HexM-GM2AP Pulldown Assay 72

4. Conclusion and Future Directions 75
5. References 78
6. Supplemental Figures 87

LIST OF TABLES

Number *Page*

1. Plasmids used in biochemical and structural analysis of HexM 25
2. Cell cultures used for HexM analysis 26
3. PCR Components..... 34
4. Thermocycling Conditions for PCR..... 35
5. Double Digest Components 36
6. HexA and HexM kinetic values for MUG and MUGS substrates 46
7. Crystallographic Statistics 59

LIST OF FIGURES

Number *Page*

1. The chemical structure of GM2 ganglioside 11
2. Model of β-hexosaminidase isozymes 13
3. M6PR-mediated transport of HexA 14
4. GM2-ganglioside processing in the lysosome 15
5. Model of the creation of HexM 21
6. HEK293T cells grown in a FiberCell Bioreactor 42
7. Western Blot of HexM 43
8. SDS PAGE gel of histidine-tagged HexM from T-75 flask and FiberCell. 44
9. The structure of MUGS 45
10. MUGS activity assay 46
11. Long-term stability experiment 47
12. Diagram of GlcNAc-1-phosphotransferase function 49
13. PCR amplification of pcDNA6/V5-His-GlcNAc-1-PT plasmid 51
14. SDS PAGE and Western Blot of HexM and phosHexM 52
15. PhosphoProtein Gel Stain image 53
16. TSD Fibroblast cellular uptake assay 54
17. MALDI-MS analysis of HexA, HexM, and phosHexM 57
18. Ribbon diagram of HexM active sites 60
19. Orientation of HexM dimer interface 61
20. Orientation of HexM monomers 62
21. Model of HexM homodimer bound to complexes of GM2A/GM2 63
22. The proposed catalytic mechanism for HexM 64
23. PCR amplification of gBlock 65
24. Enzyme restriction digest of PB-T-RfAHexM plasmid 66
25. Colony PCR results 67
26. SDS PAGE gel and Western Blot of HexM and HexME322Q mutant 68
27. Activity assay comparing MUGS hydrolysis of HexM and HexME322Q. 69

28. Negative stained specimen 70
29. Compiled Transmission Electron Microscopy (TEM) images 70
30. Average EM envelope of the HexM dimer..... 71
31. SDS PAGE and Western Blot of purified GM2AP..... 72
32. Averaged size distribution of 10 runs of 0.25mM liposome mixture 73
33. Pulldown assay of HexM-GM2AP 74

ABBREVIATIONS

α – Alpha

Å – Angstrom

A_{260} – Absorbance at 260 nm

β – Beta

BSA – Bovine Serum Albumin

ºC – Degrees Celcius

CDM-HD - Chemically Defined Media For High Density

cDNA – Complimentary DNA

CGT- Ceramide glucosyltransferase

CNS- Central Nervous System

ddH_2O – Double deionized water

DMSO – Dimethylsulfoxide

DNA – Deoxyribonucleic acid

ER – Endoplasmic reticulum

ERAD- Endoplasmic-reticulum-associated protein degradation pathway

ERT- Enzyme Replacement Therapy

g – Gram

GM2 ganglioside- GM2 mono-sialic acid substrate

GM2A - GM2 activator gene

GM2AP – GM2 activator protein

HEK293T- Human Embryonic Kidney cell line

HexA- β-Hexosaminidase A

HexM – β-Hexosaminidase M

LB- Lysogeny broth

M6P- Mannose-6-phosphate

M6PR- Mannose-6-phosphate Receptor

NOEV- N-octyl-epi-β-valienamine

SD - Sandhoff Disease

SDS-PAGE – Sodium dodecyl sulfate- polyacrylamide gel electrophoresis

TSD - Tay-Sachs Disease

WB – Western Blot

Chapter 1: Introduction

1.0 Lysosomal storage disorders

Lysosomal storage disorders (LSDs) are a group of approximately 50 diseases characterized by the pathological accumulation of metabolic waste products in the lysosome as a result of enzyme deficiencies. LSDs can be sub-categorized based on the type of substrate that is accumulated in the lysosome. One such substrate is GM2 ganglioside, an acidic glycolipid that is continuously recycled in neurons of the brain and peripheral nervous system (See Fig 1) (1) and the resulting disorders are known as GM2 gangliosidoses.

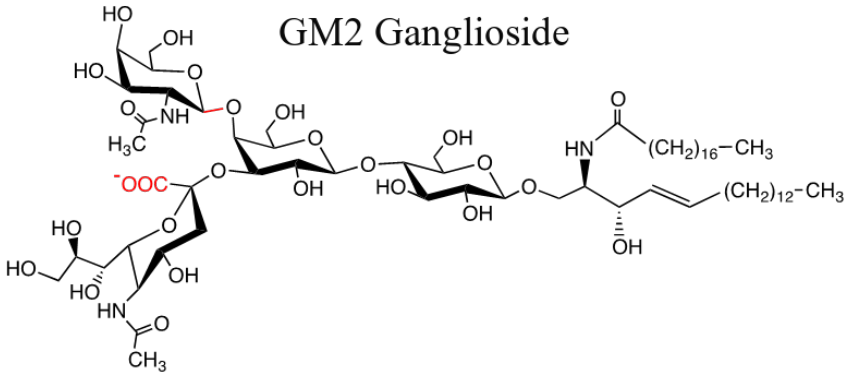

Figure 1: The chemical structure of GM2 ganglioside. The bond (in red) indicates the cleavage site of HexA. The negatively charged carboxylate group, highlighted in red, promotes the binding of the positively charged active site of GM2 activator protein (GM2AP) and the positively charged binding site on the α-subunit of HexA.

1.1 GM2 gangliosidoses

GM2 gangliosidoses are autosomal recessive neurodegenerative diseases that result from heritable loss-of-function mutations in genes *HEXA* or *HEXB*, which code for the α- and β-subunits of the lysosomal enzyme β-hexosaminidase A (HexA), respectively (2). Deficiencies in

the α- or β-subunit leads to Tay-Sachs (TSD) or Sandhoff disease (SD), respectively. The third gene involved in GM2 gangliosidosis, *GM2A*, encodes the GM2 activator protein (GM2AP). Mutations in *GM2A* also cause GM2 gangliosidosis, but they are considerably rarer than the disease-causing mutations in *HEXA* or *HEXB*. The rate of GM2 accumulation depends on how severely the mutations reduce HexA activity. Clinical disease does not develop unless residual HexA activity drops below a critical threshold of 5–10% of normal (3). Complete loss of HexA activity results in the onset of clinical symptoms during infancy, whereas mutations resulting in residual activity slows GM2 accumulation and leads to late-onset (juvenile- or adult-onset) forms of the disease.

1.2 Hex Isozymes

The α- and β- subunit of HexA each possess their own active sites, though dimerization is necessary to stabilize the site for it to function. The α-subunit has a positively charged binding site that facilitates the binding of negatively charged GM2 ganglioside (4). The β-subunit has a negatively charged binding pocket and cannot efficiently bind GM2 ganglioside (5). In normal human cells, the α- and β- monomers complex to form one of two isozymes, HexA (αβ) and HexB (ββ) (See Fig 2). In Sandhoff disease patients, a third highly unstable isozyme, HexS (αα), is found at low levels. All three isozymes possess differences in thermal stability due to sequence variations present at the dimer interface, with HexB being the most stable, followed by HexA, and HexS (5,6).

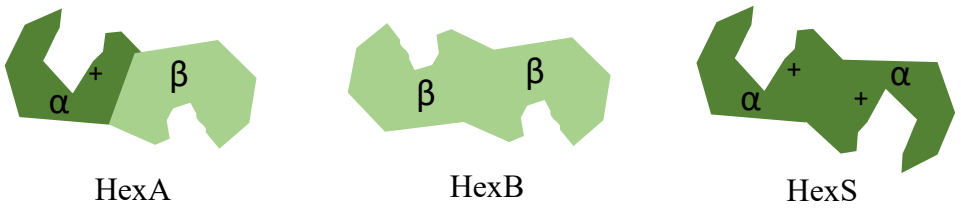

Figure 2: Model of β-hexosaminidase isozymes. The α-subunit possesses a positively charged binding pocket that efficiently binds GM2 ganglioside. The β-subunit is also capable of hydrolyzing substrates in its active site, and additionally imparts increased thermal stability in the heterodimer HexA (αβ) and the homodimer HexB (ββ). Despite possessing two α-subunit positively charged binding pockets, HexS is highly unstable and therefore insufficient in ameliorating the effects of the deficiency of the β-subunit, leading to Sandhoff disease.

The third gene involved for GM2 gangliosidosis, *GM2A*, encodes the GM2 activator protein (GM2AP). Mutations in *GM2A* also cause GM2 gangliosidosis, but they are considerably rarer than the disease-causing mutations in *HEXA* or *HEXB*.

1.3 Synthesis and Transportation of HexA

The α and β- subunits of HexA are directed to the ER by a signal peptide and co-translationally secreted into the endoplasmic reticulum (ER), where they lose their signal peptide, form intra-chain disulfide bonds, and acquire N-linked oligosaccharides. The subunits complex to form precursor HexA after this glycosylation step (7). Mannose-6-phosphate (M6P) moieties are attached in the *cis* Golgi network and recognized by specialized M6P receptor (M6PR) proteins in the *trans* Golgi network, which facilitate the targeted delivery of HexA into lysosomes. M6PR binds to M6P at a pH of 6.5-6.7, as the interior of the lysosome lowers in pH M6PR dissociates from M6P, releasing the enzyme into the lysosome (Fig 3). As with other soluble lysosomal-bound glycosidases, a significant fraction (10-20%) of the M6P-tagged

enzyme is secreted into the extracellular space and can be detected in the medium of cultured cells (8). Importantly, active extracellular HexA can be endocytosed by enzyme deficient cells via the mannose-6-phosphate receptor (M6PR) pathway and targeted to their lysozymes (9). This process, known as cross-correction, is mediated by *N*-linked oligosaccharides containing mannose-6-phosphate (M6P) that decorate the surface of lysosomal enzymes.

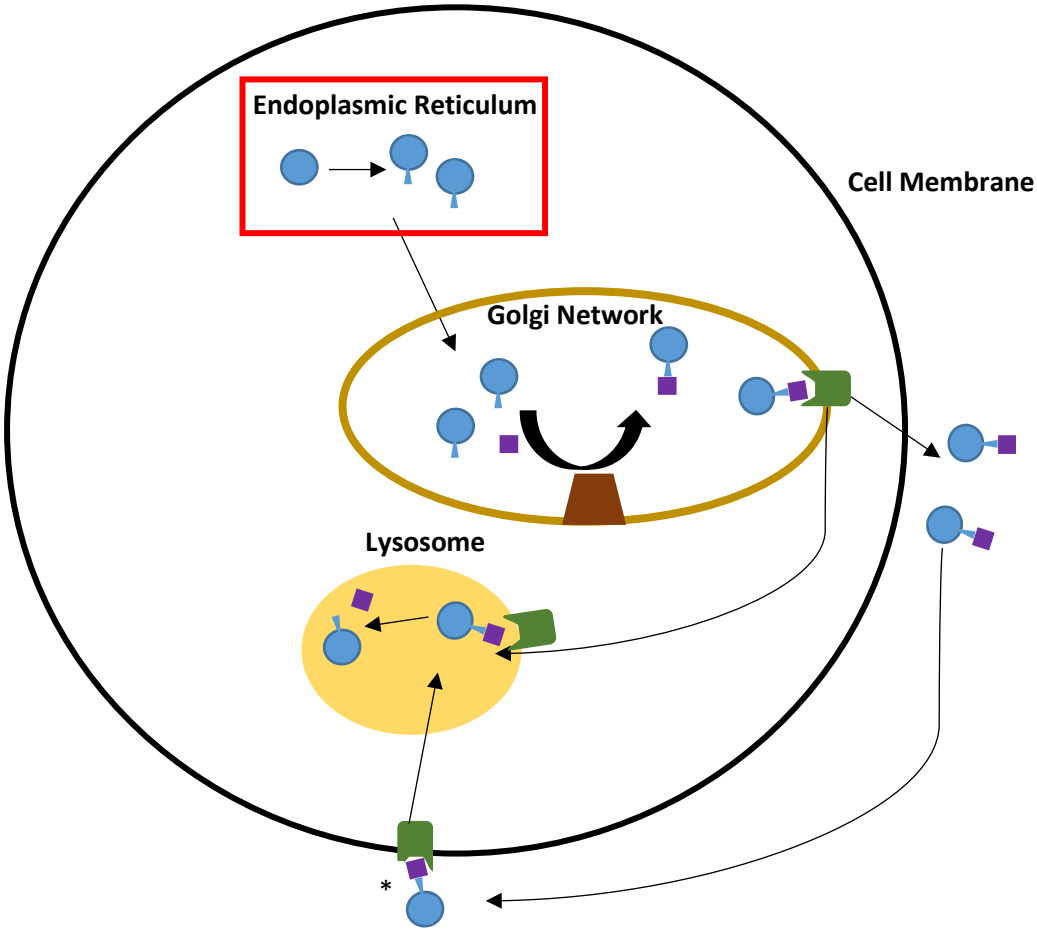

Figure 3: M6PR-mediated transport of HexA. HexA dimers (blue circles) are glycosylated (blue triangles) in the ER. GlcNAc-1-phosphotransferase (brown trapezoid) adds a mannose-6-phosphate group (purple square) to HexA in the Golgi network. Mannose-6-phosphate receptors (green) bind to the M6P group of HexA and deliver the protein to lysosomes within the cell. The lowered pH in the lysosome causes the M6PR and phosphate group to dissociate from HexA. A

portion of M6P-tagged HexA (*)secreted by the cell and can be taken up by M6P receptors that decorate the surface of neighbouring cells and subsequently targeted to the lysosome (9).

1.4 The Role of GM2AP and HexA in the Lysosome

GM2AP is a small, glycolipid-transport protein that removes a molecule of GM2 ganglioside from the lysosomal membrane and presents it to HexA for hydrolysis (10). HexA and the GM2AP-GM2 complex interact in the lysosome to form a soluble, active quaternary complex with the GM2 ganglioside substrate (GM2) correctly positioned for hydrolysis by the active site of the α-subunit of HexA (Fig 4) (11).

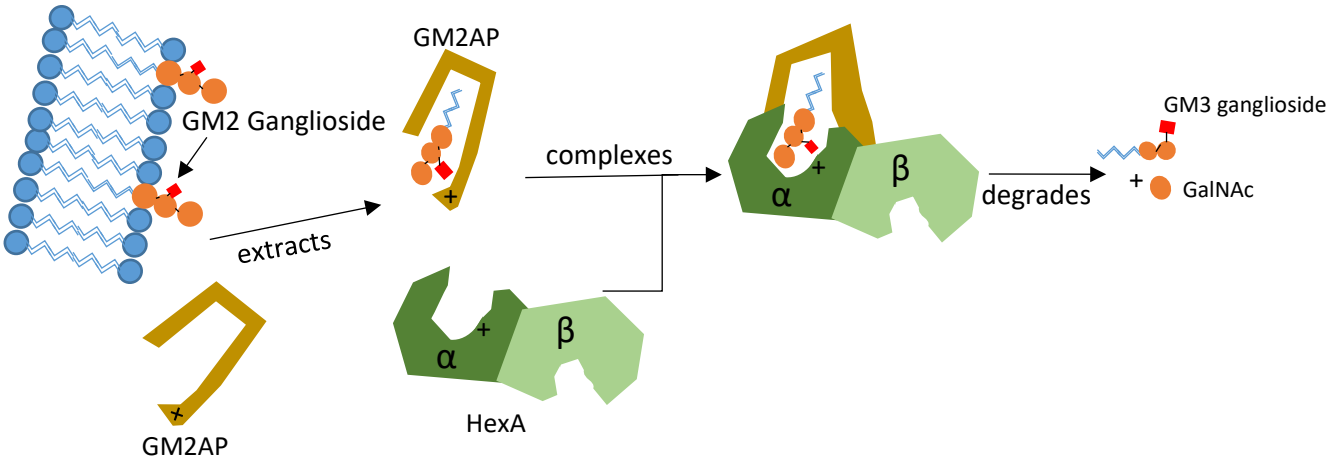

Figure 4: GM2-ganglioside processing in the lysosome. GM2-ganglioside is extracted from membrane fragments in the lysosome by GM2AP, complexed with HexA, and processed into GM3-ganglioside and N-Acetylgalactosamine (GalNAc). The negatively charged sialic acid moiety of GM2 presented by GM2AP preferentially interacts with the positively charged binding pocket of the α-subunit of HexA (11).

1.5 Genetic Screening for GM2 Gangliosidosis

Effective carrier screening programs successfully reduced the incidence of Tay-Sachs disease among higher risk populations, including eastern French Canadians (1 in 14) and Ashkenazi Jews (1 in 30), by more than 90% in the United States and Canada (12). Recently, sequence-based screening has made improvements over the standard biochemical method, a wider range of mutant HexA variants can be detected and a lowered amount of false positives can be detected, more effectively assessing an increasingly global pan-ethnic population (13). Despite the significant progress of screening methods developed to reduce the incidence of TSD and SD, GM2 gangliosidoses remain one of only a few high frequency lysosomal storage diseases without a treatment.

1.6 Animal Models for GM2 gangliosidoses

Potential therapies for the GM2 gangliosidoses have been tested in many animal models, including mouse, cats, sheep, as well as in human clinical trials with varying degrees of success (14). Mouse strains that have had their *HEXA* and *HEXB* gene expression abrogated were the initial animal models used to assess the effects of TSD and SD (15). The TSD mouse model was found to differ greatly in terms of symptoms and how the disease progressed as compared to its counterpart in human infants. In contrast, the SD mouse model developed the fatal neurodegenerative symptoms of Sandhoff Disease, dying at four to five months of age. These findings led researchers to the discovery of a biochemical bypass, Sialidase-3 (encoded by *NEU3*), which breaks down GM2 ganglioside, preventing its pathological accumulation in the brain. Recently, it was found that a TSD mouse model exhibiting human-like disease traits is possible if *NEU3* is inactivated alongside *HEXA* in mice (16).

1.7 Experimental GM2 Gangliosidosis Therapies

To prevent the pathological accumulation of GM2 ganglioside the influx of substrate into the lysosomal compartment cannot exceed the catabolic threshold of its degradative enzymes present in the compartment. Therapeutic methods must therefore either decrease the rate of ganglioside accumulation or increase the catabolic rate of the necessary lysosomal enzymes involved in its degradation. Notably, as little as 10% of normal HexA activity could prevent, and possibly reverse, GM2 accumulation and associated clinical phenotypes, making pharmacological chaperone therapy, substrate reduction therapy, enzyme replacement therapy (ERT) and gene therapy attractive possibilities for managing GM2 gangliosidoses (17).

1.7.1 Pharmacological Chaperone Therapy

In patients with adult-onset TSD, the most commonly identified allele is G269S (18). Surprisingly, G269S, as with other mutations that lead to adult-onset TSD, do not reduce the catalytic activity HexA to below the 10% critical threshold. Instead, many of these mutations have been implicated in interfering with proper folding pathways and targeting to the lysosome (19,20). *In vitro* studies have shown that G269S loses activity at physiological temperatures (21). This is thought to be caused by the serine side chain sterically hindering local backbone conformation, preventing proper folding and trafficking to the lysosome (6).

Due to the adverse effects on protein folding, the endoplasmic-reticulum-associated protein degradation pathway (ERAD) has been found to play an important role in selectively targeting HexA mutants for ubiquitination and subsequent degradation (8). OS-9, a lectin required for glycoprotein degradation, and SEL1-L, an adapter protein for an ERAD ubiquitin ligase, have been shown to selectively bind HexA α-subunit mutants (8,22,23). Since it is protein degradation as opposed to loss of catalytic activity that can drive adult-onset GM2 gangliosidosis, much work has been done to develop pharmacological chaperones that help

stabilize the HexA mutant, thereby avoiding ERAD mediated degradation and increasing delivery of the enzyme to the lysosome (24–26)

As one of the most common mutations of HexA, G269S, was a result of ERAD degradation, despite maintaining the enzyme's active site, a chemical chaperone was also studied using a GM2 gangliosidosis model (24). TSD and SD fibroblast cells from adult patients were assessed in the presence of *N*-acetylglucosamine thiazoline (NGT), a known competitive inhibitor of HexA. It was found that NGT acted in a dose-dependent manner, and at 0.9mM concentrations, acted as a HexA chaperone, increasing residual HexA activity by three-fold in a TSD fibroblast primary cell line. Pyrimethamine, a chemical originally used to treat the parasitic disease toxoplasmosis, was identified as the most potent inhibitor of HexA from a National Institute of Neurological Disorders and Stroke library of 1040 compounds approved by the Food and Drug Administration for use as chemical chaperones (25,26). The study looked at the effects of pyrimethamine on fibroblast cell lines cultured from 10 late-onset Tay-Sachs and 7 Sandhoff disease patients (26). Of the Tay-Sachs cell lines, 11 α-subunit and 2 novel mutations were identified. When grown in the presence of pyrimethamine in concentrations that correspond to therapeutic doses, cells that had the G269S α-subunit mutation, as well as 7 β-subunit mutations tested were found to have significantly increased residual HexA activity (26). Pyrimethamine concentrations above 0.1 mM were found to have an inhibitory effect on Hex activity. A clinical trial was ultimately conducted on late-onset Tay-Sachs patients by providing oral doses of pyrimethamine to a maximum of 100 mg a day (27). The study found that patients who received 50 mg a day or less had a 4-fold enhancement of HexA activity. However, the study also found that patients experienced significant side effects at or above 75 mg pyrimethamine per day, and a

study has previously found the long-term use of pyrimethamine is associated with an increased risk for cancer (28).

1.7.2 Substrate Reduction Therapy

Another possible approach to treating GM2 gangliosidosis is to reduce the amount of GM2 ganglioside being produced, thereby preventing the accumulation in lysosomes with insufficient active HexA. Glycosyltransferases play a necessary role in the sequential biosynthesis of GM2 ganglioside, following the reverse pathway of their degradation. Structural mimics of ceramide with a strong binding affinity have been found to inhibit the biosynthetic enzyme ceramide glucosyltransferase (CGT) (29,30). Towards the purpose of treating Tay-Sachs and Sandhoff diseases, a novel iminosugar, *N*-butyldeoxynojirimycin (Miglustat™), that inhibits the enzyme glucosylceramide synthase was developed (31). Miglustat has been found in human CSF after dosing, indicating that it crosses the blood-brain barrier. The medication has proven to be useful in specific situations, including stabilizing two patients with juvenile Sandhoff disease (32,33). However, a randomized 12-month study involving patients aged 18 or older found no difference on any efficacy measurement tested between the Miglustat group and the control group (34).

1.7.3 Enzyme Replacement Therapy

A preclinical study showed efficacy of ERT in Sandhoff mice, but this required direct intracranial injection of recombinant human HexA (35); and it remains unknown if this approach would be amenable to long-term clinical management of GM2-gangliosidosis. A genetically engineered HEXB was previously created for use in ERT, consisting of a β-subunit modified with amino acid sequences from the α-subunit using structure-based homology modelling (35). It

was later revealed by a separate group that the engineered HexB protein was inactive and the activity being measured was an artifact of their enzyme assay (36). The group subsequently revised their engineered HexB enzyme and now report to have a functional version (37*).* Repeated intracerebroventricular (ICV) administration of this new version of HexB, mod2B, were found to significantly prolong the lifespan of SD mice, though only marginally decreased the accumulation of GM2 ganglioside as assessed by mass spectrometry (MS) of brain slices (37).

Despite the above, two main issues continue to limit the development of an enzyme replacement therapy for GM2 gangliosidosis: 1) The instability of human HexA and inability to produce it in gram-scale qualities, 2) limited entry of HexA into the CNS due to the blood brain barrier. However, intracranial enzyme administration has been shown to be a possible method of providing HexA to reduce GM2 ganglioside accumulation in SD mouse models. Indeed, direct intracerebroventricular (ICV) administration is a proven method of drug delivery (38–40) .

A final issue regarding the large-scale production of recombinant enzyme necessary for ERT is inadequate *in cellulo* phosphorylation. This is due to endogenous levels of glycosylating and phosphorylating enzymes being incommensurate with the artificially increased production of recombinant enzyme in mammalian cells for treatment. Co-expression of recombinant proteins used in ERT (*i.e.* β-glucocerebrosidase and lysosomal α-glucosidase) with an engineered phosphotransferase produced by Dr. Kornfeld's lab has been shown to increase protein phosphorylation and cellular uptake in HeLa cells (41).

1.7.4 Creation of HexM

Previously, critical features of the α- and β-subunits of HexA were combined into a single subunit (μ) to create a stable homodimeric version of HexA, known as HexM (42). (See Fig 5)

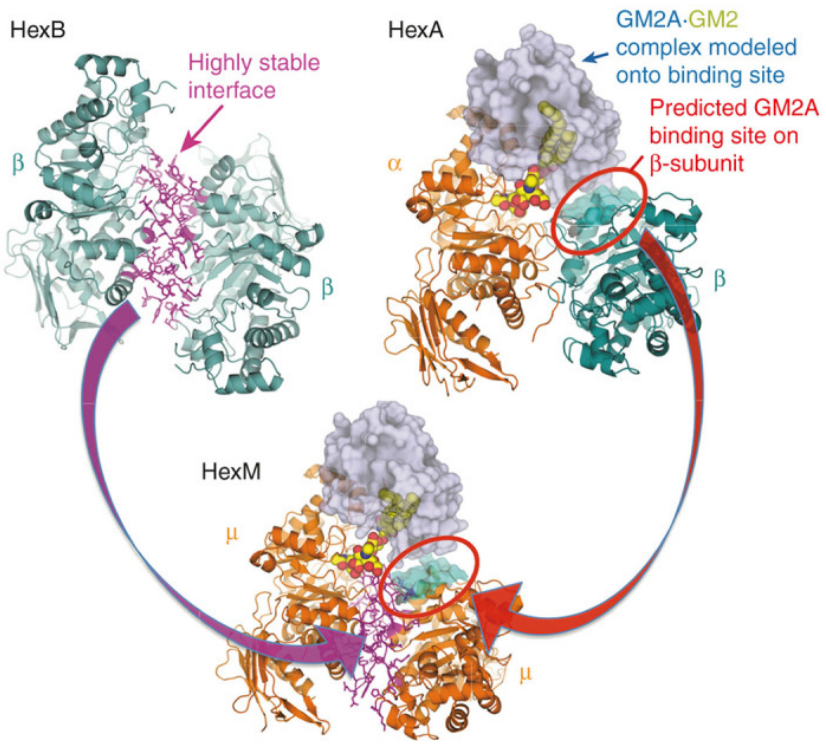

Figure 5: Model of the creation of HexM. The μ-subunit of HexM was created from the α-subunit of human HexA (orange), modified to include the stable homodimer interface (magenta) formed between the β-subunits (teal) of human HexB and areas of the β-subunit necessary for GM2AP interaction. The GM2AP (grey) bound to GM2 ganglioside (yellow spheres) was modelled onto HexA based on the solved crystal structures of HexA and HexB, and positioning was maintained for the HexM complex (5,6). Reproduced with permission of Elsevier via Copyright Clearance Center.

The goal in creating HexM was to address some of the main problems with using heterodimeric HexA for a therapeutic. As HexA consists of both an α- and β- subunit, the resulting dimer interface is more unstable than the stable homodimer HexB, potentially decreasing its efficacy in long term therapeutic trials. To address issue of stability, amino acid sequences from the β-subunit interface were included in the creation of the μ-subunit.

Furthermore, the μ-subunit retained the GM2 active site of the α-subunit, providing HexM with double the binding capacity for GM2 ganglioside. Comparison of HexA and HexM activity has found that HexM possesses double the Vmax, or maximal binding capacity, of HexA, indicating that both μ-subunit active sites may be used concurrently. Another issue regarding the production of HexA is the necessity for equal amounts of both α- and β- subunits to be produced and dimerize. The benefit of the self-dimerizing μ-subunit is that a cell line genetically engineered to produce HexM (μμ) will not produce any Hex isozymes, which would otherwise decrease the effectiveness of ERT as HexB is not as effective at processing GM2 ganglioside. The smaller packaging size of the μ-subunit also provides more opportunities for novel treatments. Gene therapy, a potentially one-time therapeutic intervention that involves specific manipulation of the DNA in enzyme deficient cells using viral vectors, is a potentially game-changing method of treating GM2 gangliosidoses. The issue with developing a gene therapy approach using HexA is the limited carrying capacity of the adeno-associated virus (AAV) (~ 4.5 kb) and the more efficacious self-complementary AAV (scAAV) (~2.1 kb) used to deliver the genetic information (43). As the DNA coding sequences for the α- and β- subunits of HexA is ~3.2 kb, AAV vectors only have the carrying capacity to deliver one of the subunits. The benefit of the μ-subunit is that no such packaging limitations exist for viral vectors, making HexM a great candidate for gene therapy.

A gene therapy study was conducted with a TSD mouse model to assess the efficacy of the μ-subunit DNA packaged into an AAV vector (44). An engineered liver-detargetted viral vector, AAV9.47, was used in the study to improve delivery to the brain and spinal cord. Previously conducted vector DNA distribution studies of AAV9.47 found it had a 110-fold decreased liver transduction compared to that of AAV9 in mice injected in the tail vein that were

analysed 4 weeks post-injection (45). Intravenous injections of scAAV9.47/*HEXM* capsid, containing a synthetic promoter to drive *HEXM* gene expression, found widespread gene transfer in all regions of the brains of adult TSD mice at 4-5 months of age as well as neonatal mice, including TSD genotype and heterozygotes. Furthermore, intravenous injection of AAV9.47/*HEXM* into neonatal TSD mice resulted in the long-term CNS reduction of GM2 ganglioside. The mice were analysed 15 months post injection and found to have half the amount of GM2/total ganglioside ratio present as compared to noninjected TSD KO control mice.

While these results are promising for the treatment of TSD, scAAV9.47/*HEXM* has also been tested in an SD mouse model (46). Intravenous injections were given to neonatal SD mice and assessed long-term for improvements in survival and behaviour. While untreated SD mice died at approximately 15 weeks, mice injected with scAAV9.47/*HEXM* had a median survival age of 40 weeks. Furthermore, behavioural tests found that injected mice outperformed their untreated age-matched counterparts and performed similarly to heterozygous controls.

Significant progress has been made in the search for treatments of GM2 gangliosidosis. The creation of HexM was a promising step, as it can be utilized through both enzyme replacement and gene therapy approaches. To fully understand the molecular basis for the remarkable enzymatic activity of HexM, a combination of molecular and structural biology methods was employed to determine the 3D crystal structure of HexM and attempts were made to form a long-lived complex of HexM bound to GM2AP. This information can be used to predict how HexM interacts with GM2AP and inform further engineering of the biochemical properties of HexM for its potential use as a biopharmaceutical to treat GM2 gangliosidosis.

1.8 Thesis objectives

As described in detail below, to advance the potential of HexM as an ERT candidate to manage GM2 gangliosidoses, I have demonstrated that the engineered enzyme is highly stable at 37^{o}C and can be purified in gram-scale quantities. Further, I demonstrate that co-expression of HexM with a modified human GlcNAc-1-phosphotransferase (41) markedly enhances the mannose-6-phosphate content on HexM and its cellular uptake into Tay-Sachs fibroblast cells. Furthermore, a crystal structure I determined of HexM, combined with mass spectrometry-based glycoform analysis, reveals how the engineering used to HexM imparts stability and GM2AP binding, yet also retains a fold and a glycosylation pattern consistent with HexA. Together, my studies advance the potential of HexM as a biologic to manage GM2 gangliosidoses.

Chapter 2: Materials and Methods

2.0 Plasmids

The HexM expression plasmids used for all stable HEK293T cell transfections were based on the *piggyBac* transposon-based cell expression system (47). The *piggyBac* plasmids were designed for the highly-efficient stable transfection of doxycycline-induced mammalian cell cultures for large-scale protein production. PBase is used to mediate the simultaneous integration, up to 14 times, of multiple transposons (PB-T-PAF or PB-T-RFA and PB-RB) into random TTAA sites of the genome of the host cell. The pcDNA plasmid was used due to its high level of expression in mammalian cells. *pcDNA6/V5-His-GlcNAc-1-PT* was developed to produce a non-selective auto-catalytic GlcNAc-1-PT capable of phosphorylating a wide range of lysosomal enzymes (48)

Table 1: Plasmids used in biochemical and structural analysis of HexM

Plasmid	Source
piggyBac Protein A Fusion (pB-T-PAF-GM2AP)[1]	Dr. Gil Privé
piggyBac Reading Frame cassette A (pB-T-RfA-HexM)[2]	Dr. Don Mahuran
piggyBac helper plasmid (pCyL43)[2]	Dr. Don Mahuran
piggyBac blasticidin S plasmid (PB-RB)[2]	Dr. Don Mahuran
pcDNA6/V5-His-GlcNAc-1-PT[3]	Dr. Stuart Kornfeld
piggyBac Reading Frame cassette A (pB-T-RfA HexME322Q)[4]	Dr. Don Mahuran
pcDNA6/V5-GlcNAc-1-PT-NoHis[5]	Dr. Stuart Kornfeld
pCI neo-hEST2.pCI neo-hEST2[6]	Dr. Bob Weinberg

[1]Used to produce Protein A-tagged GM2AP for HexM-GM2AP binding assays

[2]Used to transfect HexABKO HEK293T cells with the *piggyBac* transposon system

[3]Used to generate His-tagged GlcNAc-1-phosphotransferase for co-transfection with HexABKO-HexM HEK293T cells.

[4]HexME322Q plasmid was generated from pB-T-RfA-HexM (See Methods)

[5]His-tag on *pcDNA6/V5-GlcNAc-1-PT* was removed through site-directed mutagenesis (See Methods)

[6]Used to generate immortalized TSD Fibroblast cells for cellular uptake assay

2.1 Cell Cultures

The HEK293T cell line is a human embryonic kidney cell line derived from HEK293 cells, that expresses a mutant variant of simian vacuolating virus (SV40) large T antigen and is highly efficient for DNA transfection. The presence of SV40 large T antigen also enables transfected plasmid DNA containing a SV40 origin of replication to replicate in 293T cells and retain a high copy number, increasing the amount of recombinant protein capable of being produced. HEK293THexABKO was created using guide RNAs (gRNAs) designed to target exon

1 and exon 11 of HexA and exon 1 of HexB. HEK293T cells were co-transfected with a Cas9 nuclease expression vector and gRNAs and cells found to have no HexA or HexB activity were identified (42). HEK293TABKO-HexM-His was produced by integrating pB-T-RfA-HexM and PB-RB into the cell's genome using the *piggyBac* transposon-based mammalian cell expression system. HEK293T-GM2AP-Protein A was also produced via the *piggyBac* expression system, using the *piggyBac* plasmid pB-T-PAF-GM2AP. The protein A tag, originally from Protein A of *Staphylococcus aureus* binds to immunoglobulin G (IgG), a common human antibody Tay-Sachs disease fibroblast cells (TSD 1881) were immortalized through transfection with the SV40 T antigen and hTERT and provided by Dr. Wafa Kammouni of Dr. Barbara Triggs-Raine's lab (Biochemistry and Medical Genetics, University of Manitoba) for all cellular uptake experiments (49).

Table 2: Cell lines used for HexM analysis

Cell lines	Source
HEK293TABKO-HexM-His[1]	Dr. Don Mahuran
HEK293THexABKO[2]	Dr. Don Mahuran
HEK293TABKO-HexME322Q[3]	Dr. Don Mahuran
HEK293T-GM2AP-Protein A[4]	Dr. Gil Privé
Tay-Sachs Disease Fibroblast Cells[5] (TSD 1881)	Dr. Wafa Kammouni

[1]Used for all HexM protein production

[2]Used for transfection of HexME322Q plasmid

[3]Used for generation of HexME322Q

[4]Used to generate Protein A-tagged GM2AP for pulldown assays

[5]Used in TSD Fibroblast cell uptake assays.

2.1.1 Cell culture Media

Dulbecco's Minimal Essential Medium (DMEM) (Gibco, ThermoFisher Scientific) supplemented with 1% Penicillin-Streptomycin (PenStrep) (Gibco), doxycycline (Gibco) (1 µmol/L), and 10% Chemically Defined Media for High Density (CDM-HD) (Fibercell Systems).

50% F-12 Nutrient Mixture (Gibco, ThermoFisher Scientific)/50% DMEM supplemented with doxycycline (Gibco) (1 µmol/L), 1% PenStrep (Gibco), and 10% CDM-HD (FiberCell Systems Inc. New Market, Md)

2.1.2 Bacterial Strains

Escherichia coli (New England Biolabs; C2987U) – A chemically-competent DH5α derivative used for all plasmid DNA manipulations. Genotype: fhuA2 Δ(argF-lacZ) U169 phoA glnV44 Φ80 Δ(lacZ)M15 gyrA96 recA1 relA1 endA1 thi-1 hsdR17

2.1.3 Bacterial Culture Media

Lysogeny Broth (LB) (Millers, Maryland, USA) – Was used for culturing *E. coli*. This consisted of 10g tryptone (Gibco, ThermoFisher Scientific), 5g yeast extract (Gibco), and 10g NaCl for 1L. Autoclave at 121°C for 15 minutes. LB + ampicillin broth contained ampicillin (100µg/ml) added to the broth once it had cooled below 50°C.

LB Agar (Millers, Maryland, USA) – Was used for all transformations and consisted of LB broth with the addition of 12g agarose for 1L formulation (Sigma-Aldrich; CAS:9012-36-6). Plates

were poured once the solution had cooled to below 50°C. Ampicillin (100µg/ml) was added to LB Agar plates as described above.

S.O.C. Medium (Invitrogen, ThermoFisher Scientific, Cat# 15544034) – Was used for recovery step in *E. coli* transformations

2.2 HexM production

A *HEXA* and *HEXB* knockout HEK293T cell line (HEKHexABKO), provided by Dr. Don Mahuran (Hospital for Sick Children, Toronto), was previously stably transfected with a HexM expression construct containing a His-tag to generate HEKHexABKO-HexM (42). The HEKHexABKO-HexM cell line was seeded into a FiberCell bioreactor (C2011) following the manufacturer's protocol (FiberCell Systems Inc. New Market, Md). The seeded cells were grown in Dulbecco's minimal essential medium (DMEM) (Gibco, ThermoFisher) in the presence of 1% Penicillin-Streptomycin (Gibco), doxycycline (1 µmol/L), and 10% Chemically Defined Media for High Density (CDM-HD) (FiberCell Systems). FiberCell Systems Inc. standard protocol was followed for extraction of media from the bioreactor every two days (FiberCell Systems Inc.). His-tagged HexM was purified from the harvest via immobilized metal affinity chromatography (HisPurTM Ni-NTA resin (Thermofisher) Cat #: 88222). The wash buffer (BT buffer) used was 10mM Bis-Tris (pH 6) and 150mM NaCl. The elution buffer used was BT buffer (pH 6) and 150mM imidazole. HexM was purified by size exclusion chromatography (SEC) using BT buffer (HiLoad 16/600 Superdex 200, GE Life Sciences). The purity of HexM was determined by SDS-PAGE followed by Coomassie blue staining, as well as by western blotting by transferring a replica gel to nitrocellulose membrane followed by protein detected using an anti-HexA Rb polyclonal antibody (1/300 dilution (Abcam; ab91624).

2.2.1 HexM Activity Assay

Enzyme activity of HexM was assessed via a previously established HexA activity assay (24). Concentrated HexM purified in Bis-Tris Buffer (10mM Bis-Tris (pH 6), 150 mM NaCl) was diluted to a working concentration of 1nM in McIlvaine citrate-phosphate buffer (CP buffer; pH 4.2) supplemented with w/v 0.5% bovine serum albumin (BSA). Background activity of BSA was found to be negligible. CP buffer at a specific pH is formulated by mixing stock concentrations of 0.2M Na_2HPO_4 and 0.1M citric acid (50). Purified recombinant HexA, also expressed in the HEKHexABKO cell line (42) was provided by my lab mate Kristen Bouma for use as a positive control. 4-methylumbelliferyl-2-acetamido-2-deoxy-β-D-glucopyranoside-6-sulfate (MUGS) (Toronto Research Chemicals; M335000) was diluted in additional CP buffer supplemented w/v 0.5% BSA to produce a 6mM working solution. 10 ul of 1nM HexM was aliquoted into a 96-well plate and differing concentrations of MUGS substrate were added to a total well volume of 100 µl. Pipetting up and down was used to mix each well three times. The plate was read using a SpectraMax ID5 plate reader at 37°C. The assay was run in triplicate using the fluorescence setting (Excitation: 365 nm, Emission: 450 nm) for 30 minutes. HexA and HexM activity with 4-methylumbelliferyl-2-acetamido-2-deoxy-β-D-glucopyranoside (MUG) (Toronto Research Chemicals; M334475), a neutrally charged un-sulfated version of MUGS, was also examined. Michaelis-Menten plots of HexM and HexA activity were created using the software Prism 8 (GraphPad).

2.2.2 Long-term stability Assay

Purified HexM was diluted to 1nM in labelled PCR tubes using phosphate buffer, formulated by mixing 1M stock concentrations of NaH_2PO_4 and Na_2HPO_4 and adjusting the pH to 5.5 or pH 7 with phosphoric acid (Sigma-Aldrich; 7664-38-2) (Cold Spring Harbor). The

protein samples were incubated in 200 µl strip tubes at 37ºC over the course of two weeks. Samples were collected every 2 days and stored at -20ºC over the course of the experiment. Enzyme activity was then assessed via HexM activity assay, as described above.

2.3 Histidine Tag Removal from a N-acetylglucosamine-1-phosphotransferase plasmid

The plasmid pcDNA6/V5-His-GlcNAc-1-PT expresses a GlcNAc-1-PT that has been shown to hyperphosphorylate co-expressed lysosomal proteins and thereby enhance their cellular uptake (41). It was provided to our lab by Dr. Stuart Kornfeld (Department of Medicine, Hematology and Oncology, Washington University School of Medicine in St. Louis). The His tag was removed from the GlcNAc-1-PT plasmid in order to improve purification of co-expressed HexM from the HexABKOHexM HEK293T cell line. Chemically competent DH5α *E. coli* stock of the GlcNAc-1-PT plasmid was produced following the previously described protocol for transformation. The plasmid (6805bp) was PCR amplified using Q5 High-Fidelity DNA polymerase (M0491, New England BioLabs Inc.) following the previously described PCR protocol. The sequence of the forward primer was 5'- TGA GTT TAA ACC CGC TGA TCA G -3' (Integrated DNA Technologies (IDT)). The sequence of the reverse primer was 5' – ACC GGT ACG CGT AGA ATC GAG -3' (IDT). The Tm used for the PCR reaction was 66ºC. In order to digest the template DNA, 1µl of Dpn1 (NEB, Cat# R0176S) was added to the PCR product mixture. The tubes were incubated for sixty minutes at 37ºC. The resulting PCR product was run on a 1.2% agarose gel.

The purified gel extraction product was ligated with Instant Sticky-End Ligase Master Mix (NEB, M0370L). 47ng of the plasmid was added to a PCR tube containing 5µl 2x Ligase Master Mix and RNA-free H2O was added to a volume of 10µl. The ligation reaction was incubated at 20ºC for 30 minutes.

5µl of the ligation reaction product was added to 50µl of competent dH5α *E. coli* (NEB) in PCR tubes on ice. A negative control of *E. coli* with dH2O was also produced. After 30 minutes, the tubes were transferred to a thermal cycler set to 42ºC for 30 seconds. The tubes were then put back on ice for 5 minutes. Each tube containing 55µl of heat-shocked *E. coli* mixture was added to 300µl S.O.C. Medium (ThermoFisher Scientific, 15544034) The tubes were incubated at 37ºC for 1 hour at a speed of 225 rpm.

Bacteria from each tube were plated on LB agar plates containing ampicillin (100µg/ml) in 25 and 50 µl aliquots via spread plate technique and grown overnight at 37ºC. Colonies were found on the plasmid-transformed *E. coli* plates, while none were found on the negative dH2O control plate. Colonies were picked for overnight growth in 3ml tubes of LB + Amp broth at 37ºC. Additional bacteria were stored at -80ºC as glycerol stocks, consisting of the LB + Amp Broth with the addition of (w/v) 50% glycerol. Purified plasmid (691.5 ng/µl) collected from the bacterial colonies using a QIAprep Spin Miniprep Kit was assessed via NanoDrop and found to have an A260/A280 of 1.91 and an A260/A230 of 2.35. The deletion of the His-tag on the plasmid was confirmed by DNA sequencing using the GlcNAc1-PT-NoHis primers (See Supplementary material 1).

2.4 HexM Phosphorylation Analysis

HexM-producing HEK293T (HexABKO) cells were transiently transfected with a pCDNA6/His-tagged GlcNAc-1-phosphotransferase (GlcNAc-1-PT-NoHis) expression plasmid that was modified through site-directed mutagenesis to remove it's His tag (41). Polyethylenenimine (PEI) was used to transfect HexMHEK293T cells with the GlcNAc-1-PT-NoHis plasmid following a previously established protocol (51). 20 µg of GlcNacPT-1 plasmid was mixed with 1 ml serum-free DMEM and 60 µl of PEI and subsequently added to a T75

flask. Media from GlcNAc-1-PT transfected HEK293T cells growing in T75 flasks was collected over four days. Media from non-transfected and transfected cells were collected and purified via IMAC and SEC.

2.4.1 Cellular uptake assay using Tay-Sachs Disease (TSD) fibroblasts

A cellular uptake assay was conducted, following a modified version of a previously described protocol (41). TSD fibroblast 1881 cells (1.0 x 106 CFUs/ml), provided by Dr. Barbara Triggs-Raine (Biochemistry and Medical Genetics, University of Manitoba), were grown in 6 well plates in Dulbecco's Minimal Essential Media (DMEM) supplemented with 10% fetal bovine serum (FBS) and doxycycline (1mg/ml). Mannose-6-phosphate (Sigma-Aldrich, M3655) and mannose were added to the appropriately labelled well plates at 5mM final concentration. 25 µg of HexM phosphorylated protein was then aliquoted into each well. Cells grew overnight at 37ºC. Cells were washed with phosphate-buffered saline (PBS; pH 7.4) (Gibco, ThermoFisher Scientific) three times and the cells were subsequently scraped into an Eppendorf tube and pelleted via centrifugation (10 mins x 10,000 rpm). 100 µl of cell lysis buffer (PBS w/v 0.5% Triton-X 100) was added to each cell pellet and each tube was then placed on ice for 10 minutes. The cell lysate was pelleted using centrifugation (15 mins x 13,000 rpm) and the supernatant was collected. A MUGS activity assay was conducted on the cell lysate samples. Total protein concentration was calculated using a BSA standard curve (0 – 20 µg/ml BSA). Substrate formation was normalized by using a 4-methylumbelliferone (Sigma-Aldrich, M1381) standard curve (20 – 1000 nM).

2.5 Mass Spectrometry Analysis

All work using mass spectrometry was conducted with the assistance of Taylor Battellino and Tyler Tran working in Dr. Helene Perrault's lab (Chemistry, University of Manitoba).

Protein in 50 mM ammonium bicarbonate (pH 8.5) was digested with pepsin (pH 2.5) or trypsin (pH 8). Peptides and glycopeptides were fractionated on C18 cartridges and analyzed by MALDI-MS and HPLC-MS/MS. Fractions containing high mannose glycopeptides were analyzed by MALDI-MS/MS. Data were processed with X!Tandem for protein identification and manually for the analysis of MS/MS spectra of mannosylated and phospho-mannosylated peptides.

2.6 Transmission Electron Microscopy Imaging

Purified HexM protein concentrated to 1.5 mg/ml in phosphate buffered saline (PBS) (pH 7.0) was imaged with a FEI Tecnai F20 transmission electron microscope (TEM) operating at 200 kV by Dr. Daniel R. Beniac and Ms. Shannon Hiebert (National Microbiology Laboratory, Winnipeg, Manitoba) via negative staining using a previously described method ([52]). A carbon graphite-coated thin copper disc was glow discharged, by placing it in the vacuum chamber of a vacuum evaporator and running a current through the system to ionize the outer surface of the disc. Protein was carefully deposited onto the surface of the grid followed by staining with a 2% ammonium molybdate solution, to differentiate protein from the background.

2.7 HexM crystallization and X-ray crystallographic structure determination

Purified HexM (10mg/ml) was crystallized in 16% PEG 8000, 0.04M KH2PO4, 20% Glycerol, and 10mM betaine hydrochloride by hanging drop method. Short rectangular crystals (space group *P*21) appeared after about a month at 20ºC from 4 µl hanging drops. Crystals were taken directly from the crystallization solution and mounted on a goniometer. X-ray diffraction data for HexM crystals were collected using a Rigaku 007HF MicroFocus X-ray generator and R-AXIS IV++ detector. Data was collected from a single crystal of HexM held at 100 K in an N2 (g)

stream. Diffraction data for the HexM crystal was integrated and scaled using XDS (53), followed by merging using Aimless within the CCP4 software suite. Initial phase estimates were determined via molecular replacement within phenix.phaser using the previously determined HexA crystal structure (PDB ID: 2GK1) (6). Model building and refinement were performed using Coot and phenix.refine, respectively (54,55)**.** The structure of HexM was solved at a resolution of 2.8 Å and refined to a Rwork of 0.27 and a Rfree of 0.32. Structural images were taken using PyMOL.

2.8 Production of HexME322Q (loss of function mutant)

A pB-T-RFA (47) HexM-containing plasmid was digested using restriction enzymes AflII (R0520S) and Afe1 (R0652S) following the manufacturer's protocol (New England Biolabs Inc.). An 861 bp synthetic double-stranded DNA fragment (gBlock, Integrated DNA Technologies) (See Supplementary Figure 2) containing the single amino acid substitution (E322Q) was PCR amplified following the manufacturer's Q5 High-Fidelity (HF) polymerase protocol (New England Biolabs, M0491) (Table 3). This protocol was followed for all subsequent PCR reactions. Agarose and SDS PAGE gels were imaged using a Gel Documentation System (Axygen, Corning, Life Sciences). Thermocycling conditions varied for each PCR based on the length of the DNA sequence and Tm calculated for each set of primers (Table 4)

Table 3: PCR Components

PCR Components	25 µl reaction (µl)	Final Concentration
5x Q5 Reaction Buffer	5	1X
10mM dNTPs	0.5	200 µM
10µM forward primer	1.25	0.5 µM

10µM reverse primer	1.25	0.5 µM
Template DNA	-	0.02 U/µl
Q5 HF DNA Polymerase	0.25	1x
RNA-free H2O	to 25	-

The sequence of the forward primer was 5'- GCT GGA CAC TAG CCG CCA TTA TC -3' (Integrated DNA Technologies (IDT). The sequence of the reverse primer was 5' – GTT CGA CTT TGT AGA ACT TCC TC -3' (IDT). The Tm used for the PCR reaction was 64ºC. Agarose gel electrophoresis was used to verify PCR amplification of the gBlock (794 bp). A standard agarose gel recipe was used for all experiments, consisting of 0.6g of agarose mixed with 50ml 1x Tris-acetate-EDTA (TAE) buffer to produce a 1.2% agarose gel. 1x TAE Buffer was diluted from a 50x TAE buffer lab stock, made up of 242g Tris-base, 57.1 ml acetic acid, 100ml 0.5M sodium EDTA, with dH2O added to a final volume of 1L.

Table 4: Thermocycling Conditions for PCR

Step	Temperature	Time
Initial Denaturation	98ºC	30 seconds
30 cycles	98ºC	10 seconds
	*50-72ºC	20 seconds
	72ºC	30 seconds/kb
Final Extension	72ºC	2 minutes
Hold	4ºC	-

*Temperature for each PCR was based on the Tm calculated for each primer using NEB Tm Calculator.

A QIAquick PCR Purification Kit (Qiagen, Cat# 28104) was used on the PCR product after confirming the expected band size (~800 bp), following the recommended protocol.

A restriction digest using the enzymes AflII and AfeI was conducted on the PB-T-RfA-ABKOHEXM plasmid. These enzymes were chosen for their single site specificity within the HexM insert. The reaction took place in labelled PCR tubes, with a final volume of 20 µl (See Table 5). In preparation for ligation, a similar restriction digest was conducted with the purified gBlock PCR product, the only difference being the amount of DNA added, to a final concentration of 2.5 µg.

Table 5: Double Digest Components

Reaction Ingredients	Starting Concentration	Volume added (µl)	Final Concentration
PB-T-RfA-HEKABKOHexM	615.5 ng/µl	4	2.5 µg
CutSmart® Buffer	10x	2	1x
AfeI	10,000 units/ml	2.5	25 units/ml
AflII	20,000 units/ml	1.25	25 units/ml
RNA-free H2O	-	to 20 µl	-

Following the double digest, the plasmid was loaded in excess into an agarose gel and extracted for subsequent purification. A gel extraction kit (Qiagen; 28115) was used to clean up the extracted gel fragment.

The gBlock insert and the double digested PB-T-RfA-ABKOHEXM plasmid were then ligated with Instant Sticky-End Ligase Master Mix (New England Biolabs, M0370L). A 1:3

molar ratio of insert (gBlock, 34ng) to vector (PB-T-RfA plasmid, 100ng) was added to a PCR tube containing 5µl 2x Ligase Master Mix and RNA-free H2O was added to a final volume of 10µl. The ligation reaction was incubated at 20ºC for 30 minutes.

5µl of the ligation reaction product was added to 50µl of chemically competent dH5α *E. coli* (New England Biolabs; C2987U) in PCR tubes on ice. A negative control of *E. coli* with just dH2O and a plasmid control of *E. coli* with the vector was also produced. After thirty minutes, the tubes were transferred to a thermal cycler set to 42ºC for 30 seconds. The tubes were then put back on ice for 5 minutes. Each tube containing 55µl of heat-shocked *E. coli* mixture was added to 300µl S.O.C. Medium (ThermoFisher Scientific, 15544034) The tubes were incubated at 37ºC with a shake speed of 225 rpm for 1 hour.

Bacteria from each tube were plated on LB agar plates containing ampicillin (100µg/ml) in 25 and 50 µl aliquots via spread plate technique and grown overnight at 37ºC. Seven colonies were picked from the vector with insert plate into separate PCR tubes containing RNA-free H2O. A colony PCR was conducted, using the previously described gBlock PCR thermocycling conditions with the addition of an initial 90 seconds at 95ºC to heat lyze the bacterial colonies.

Colonies with the largest amount of PCR product were selected for overnight growth in 3ml tubes of LB+Amp broth at 37ºC. Excess bacteria were stored at -80ºC as glycerol stocks, consisting of the LB+Amp Broth with the addition of (w/v) 50% glycerol (Sigma-Aldrich, G5516).

The transformed plasmid (PB-T-RfA-HEXME322Q), containing a single amino acid substitution, was confirmed by DNA sequencing using the previously described gBlock primers (See Supplementary Material 3).

2.8.1 HexME322Q HEK293T Cell Transfection

The modified PB-T-RfA-HEXME322Q was transfected into HexABKO HEK293T cells using a Gateway *piggyBac* transposon expression system, previously used to transfect HEXM into HexABKO HEK293T cells (42,47).

The HexME322Q plasmid contained His-tagged HexME322Q cDNA under the control of a tetracycline inducible promoter and a puromycin selectable marker. pBASE, a self-expressing plasmid containing the *piggyBac* transposase used for transposon mediated genomic integration, and PB-RB, a *piggyBac* plasmid containing a reverse tetracycline transactivator and a blasticidin S resistance gene, were mixed with the PB-T-RfA HexME322Q plasmid in a 1:1:8 DNA ratio. The transfection was carried out using polyethylenenimine (PEI) (Sigma-Aldrich, 765090) following a previously established cell transfection protocol ([51]). HexABKO HEK293T cells were added to Nunc™ EasYFlask™ T-75 flasks (ThermoFisher; 156472) and allowed to grow overnight to confluency prior to the transfection. The plasmid mixture was added to serum-free DMEM cell media in an Eppendorf tube. PEI was then added to the Eppendorf tube in a 3:1 volumetric ratio, calculated based on the total volume of the three plasmids added. The mixture was incubated at 20ºC for 30 minutes. PEI-DNA mixture was added to each T-75 flask containing confluent HexABKO HEK293 cells in a drop-wise fashion.

The stably transfected HEK293T cells grew for three days at 37ºC in selective media, comprised of DMEM media with the addition of Puromycin (2 µg/ml) (ThermoFisher) and Blasticidin S (2 µg/ml) (ThermoFisher). Media was collected and protein was purified via IMAC and SEC, then confirmed by western blot.

2.9 GM2AP production

HEK293T cells, transfected with the *piggyBac* plasmid PB-T-PAF-GM2AP to produce Protein A-tagged GM2AP, were provided by Dr. Gil Privé. The cells were seeded into a FiberCell bioreactor, following the standardized procedure (FiberCell Systems Inc.). Cells were grown in 50% F12/50% Dulbecco's Modified Eagle Medium (DMEM) supplemented with doxycycline (1 μmol/L), 1% PenStrep (Gibco), and 10% CDM-HD (FiberCell Systems Inc. New Market, Md). FiberCell Systems Inc. standard protocol was followed for the extraction of media from the bioreactor every two days.

Protein from the collected media was resolved using an IgG Sepharose 6 Fast Flow affinity column using 25mM HEPES (pH 7.5), 150mM NaCl (IgG binding buffer). After overnight incubation with His-tagged TEV protease (New England Biolabs, P8112S) (100ug/ml resin), protein was eluted with IgG binding buffer. Fractions containing GM2AP were pooled and loaded onto a Ni-NTA column to remove TEV protease. Fractions were collected and further purified via SEC on a S75 column in 5mM Tris-HCl, 50mM NaCl (pH 7.0). Purified GM2AP was assessed via SDS PAGE and Western Blot.

2.9 Production of Intraendolysosomal-like Liposomes

Lyophilized cholesterol (Sigma-Aldrich; C8667) and GM2 ganglioside ((2S,3R,4E)-3-Hydroxy-2-(octadecanoylamino)octadec-4-en-1-yl 2-acetamido-2-deoxy-β-D-galactopyranosyl-(1→4)-[5-acetamido-3,5-dideoxy-D-glycero-α-D-galacto-non-2-ulopyranonosyl-(2→3)]-β-D-galactopyranosyl-(1→4)-β-D-glucopyranoside) were solubilized in chloroform. Lyophilized GM2 ganglioside originating from the brain of a deceased TSD child was provided by Drs. Michael Tropak and Don Mahuran. A previously established procedure to produce GM2-containing neuronal liposomes was used (56). Lipid concentration of the intraendolysosomal-like vesicles was 0.5 mM. Soluble lipids mimicking the lipid composition in neuronal

intraendolysosomal vesicles were formulated with 5mol% cholesterol (Sigma-Aldrich, CAS#57-88-5), 20 mol% BMP (bis(monooleoylglycero)phosphate (S,R Isomer) (ammonium salt)) (Avanti Polar Lipids, Alabama, 857133) , and 2 mol% GM2 ganglioside. Liposomes not containing GM2 ganglioside were made with an additional 2 mol% DOPC to compensate. Excess chloroform and methanol were evaporated from the lipid mixture under a speed vacuum (Savant SpeedVac, ThermoFischer Scientific, SPD120) for 45 minutes. The lipid pellet was solubilized in 1mL CP buffer (pH 4.2) and subjected to eight cycles of freeze-thaw with liquid nitrogen, producing a cloudy suspension. The lipid suspension was then passed through 100nm polycarbonate filters in a mini-extruder (Avanti Polar Lipids, Alabama) 21 times, following the manufacturer's recommendation.

2.9.1 Dynamic Light Scattering Analysis

40 µl of liposome sample, produced as described above, was aliquoted into a disposable micro cuvette (Malvern Panalytical, ZEN0040) and analyzed with a Zetasizer Nano-S Dynamic Light Scattering (DLS) instrument (Refractive index: 1.45, Abs: 0.001).

2.10 HexM-GM2AP Pulldown Assay

Purified GM2AP (150 µg) was incubated in the presence of GM2-containing liposomes, Nos-GM2-containing liposomes, or no liposomes, (50 µl) in CP buffer (pH 4.2) at 37°C for 30 minutes. HexM (75 µg) was added to 15µl equilibrated Pierce™ Ni-NTA Magnetic Agarose Beads (1mg protein/15µl resin) (ThermoFisher Scientific, 78606) in CP buffer and incubated with shaking (37°C, 150 rpm) for 30 minutes. HexME322Q was also studied under the same conditions. The GM2AP-liposome mixture was added to HexM-loaded beads and incubated with shaking (37°C, 150 rpm) for 1 hour. The Ni-NTA beads were washed for 60 seconds with 200 ul

pulldown buffer (CP Buffer (pH 4.2), 20 mM NaCl, 0.05% w/v Tween-20) three times. Samples were taken between each wash step. Protein was eluted using 50 µl elution buffer (CP buffer (pH 4.2), 20mM NaCl, 0.05% w/v Tween-20, 250mM Imidazole). Bands were visualized via SDS PAGE that was visualized using a Gel Documentation System (Axygen, Corning, Life Sciences).

Chapter 3: Results and Discussion

3.1.0 Production and biochemical analysis of HexM

To use HexM for enzyme replacement therapy, it must be easily produced in large quantities. To demonstrate this goal in the laboratory, a FiberCell bioreactor system was used to grow gram-scale quantities of HexM and found to be a useful, scalable, alternative to traditional methods of flask culturing. HexM MUGS activity was tested and compared to that of lab-grown HexA, producing Michaelis-Menten kinetics consistent with previously conducted biochemical analysis (42). HexM was also found to be stable in phosphate buffer (pH 5.5 and 7) for at least two weeks at 37ºC, highlighting the potential for long-term sustained activity in its therapeutic application. The results of these efforts are detailed below.

3.1.1 Increasing the production of HexM

A HEK293T cell line lacking endogenous Hex activity (HEKHexABKO) was previously stably transfected with a His-tagged HexM expression construct to generate HEKHexABKO-HexMHis (42). This cell line was seeded into a FiberCell bioreactor (FiberCell Systems). The hollow fibers of the FiberCell act like a capillary system, allowing for the removal of waste products without disturbing the cells (Figure 6). The 4000 cm^2 surface area of the FiberCell

cartridge provides a 3-dimensional growth matrix that allow cells to survive anywhere within the cartridge to a maximum cell density of $10^9/4000cm^2$ (FiberCell Systems).

Figure 6: HEK293T cells grown in a FiberCell Bioreactor. The black arrow indicates the direction of media flow within the cartridge. Cells are located within the cartridge, surrounded by hollow fibers. Clumps of dead cells are routinely removed via media collection.

Media was collected from the bioreactor every two days and frozen at -80ºC. HexM was purified from pooled frozen extracts as needed via immobilized metal affinity chromatography (IMAC) and size exclusion chromatography (SEC). The presence of HexM was determined by western blotting using an anti-HexA Rb polyclonal antibody (1/300 dilution (Abcam; ab91624). (See Figure 7).

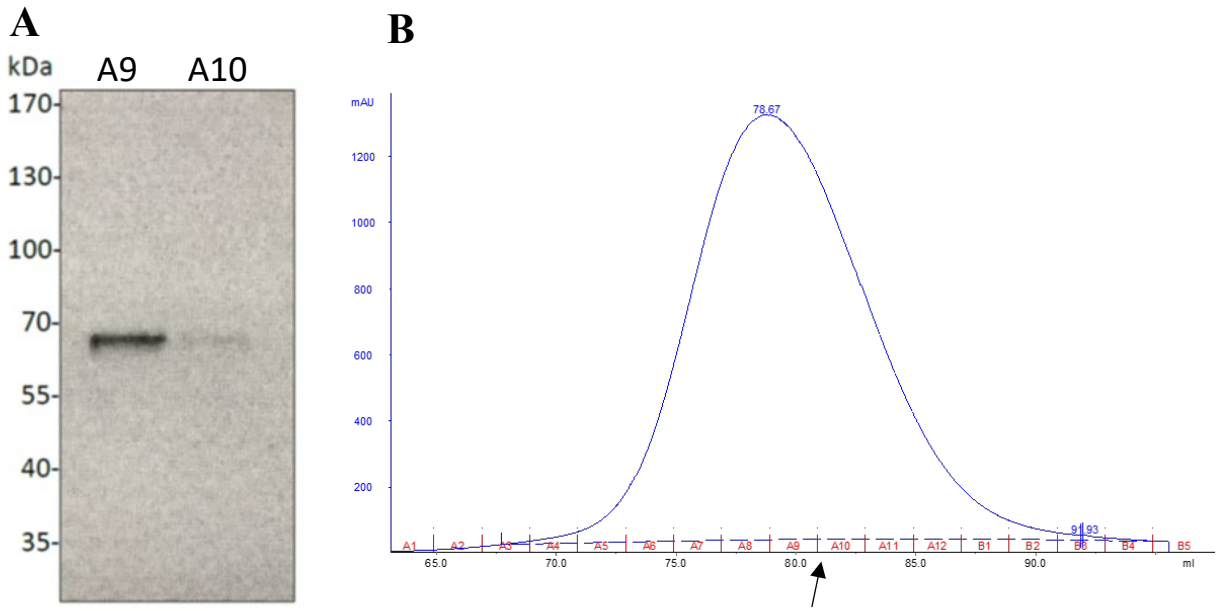

Figure 7: Western Blot of HexM. Fractions were collected from a HiLoad 16/600 Superdex 200 (GE Life Sciences) gel filtration column. A. 50µl of each sample was taken from FPLC fractions (A9 and A10) and assessed for the presence of the HexM in its reduced form (~62kDa). An anti-HexA antibody was used to detect the protein (ab91624). B. Chromatogram of a S200 gel filtration column run, the fractions tested by western blot are indicated by the black arrow.

Purification of media harvests collected from the bioreactor had an average yield of ~3 mgs of protein every two days, a 7-fold increase compared to conventional flasks, which produced 1.2 mgs from the combined media of twenty T-75 flasks over seven days (See Figure 8).

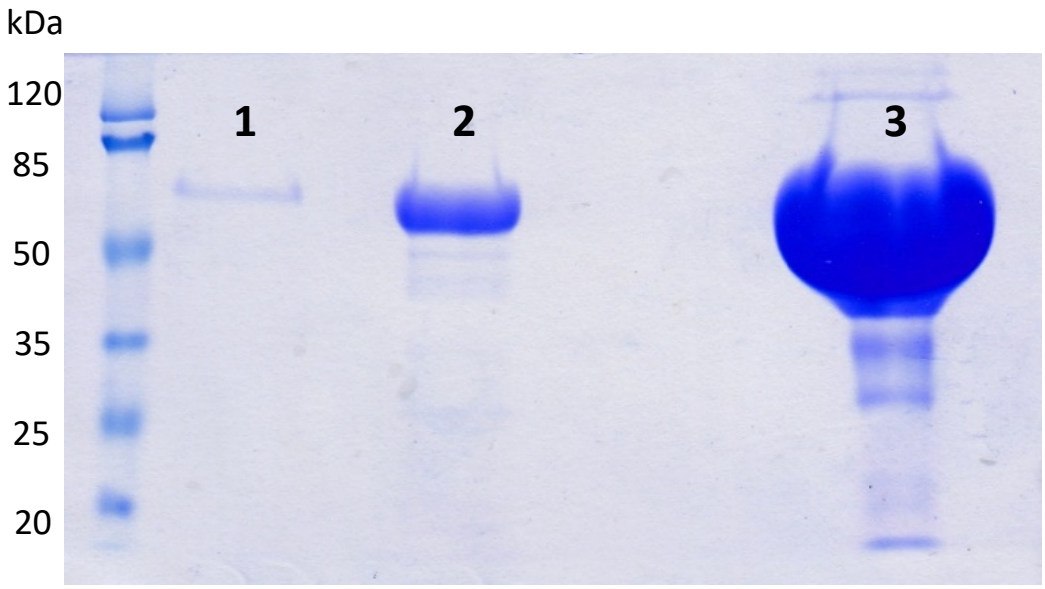

Figure 8: Coomassie Blue Stained SDS PAGE gel of histidine-tagged HexM (~68 kDa) from T-75 flask and FiberCell. Protein produced from stably transfected human embryonic kidney cells lacking endogenous *HEXA* and *HEXB* genes (HEK293T-ABKO). Well 1 was a sample taken from a suspension flask. Wells 2 and 3 were samples taken from the same FiberCell harvest. Well 2 is a 1 in 20 dilution of the purified protein. Well 3 is an undiluted sample of the purified protein.

The bioreactor was run for 150 days, yielding an estimated total of 250 mg of HexM protein. Larger FiberCell cartridges, with a surface area of $1.2m^2$ and a maximum cell density of $5x10^{10}/1.2m^2$ are available and can be run in parallel. Given the yields from the medium sized cartridge used in this study, 30 mg/week could easily be generated using 2 or 3 large cartridges in tandem. Given these yields, HexM could clearly be generated in gram quantities if industrial-scale bioreactor system were employed. This is a particularly exciting result the yields are in-

line with what would be needed to employ recombinant HexM as an enzyme replacement therapy in the clinic.

3.1.2 MUGS Activity Assay

MUGS is a synthetic fluorogenic substrate that possesses a negatively charged sulfate group, mimicking the electrostatic interaction between GM2 ganglioside and the α subunit in wild-type HexA (Figure 9).

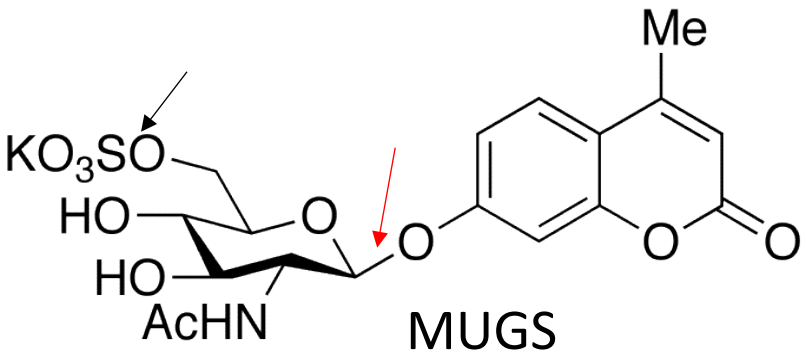

Figure 9: The structure of MUGS. The negatively charged sulfate group of MUGS mimics GM2 ganglioside's carboxylate group (black arrow), that promotes interaction with the positively charged binding pocket of HexA **(**57**)**. The chemical bond cleaved by HexM is shown (red arrow).

When cleaved by a β-hexosaminidase, the resulting fluorescent moiety 4-methylumbelliferone (4MUB) can then be detected by plate reader. Enzyme activity of HexM and HexA was assessed via a MUGS activity assay, and corroborated previously established biochemical data (See Figure 10) (42)

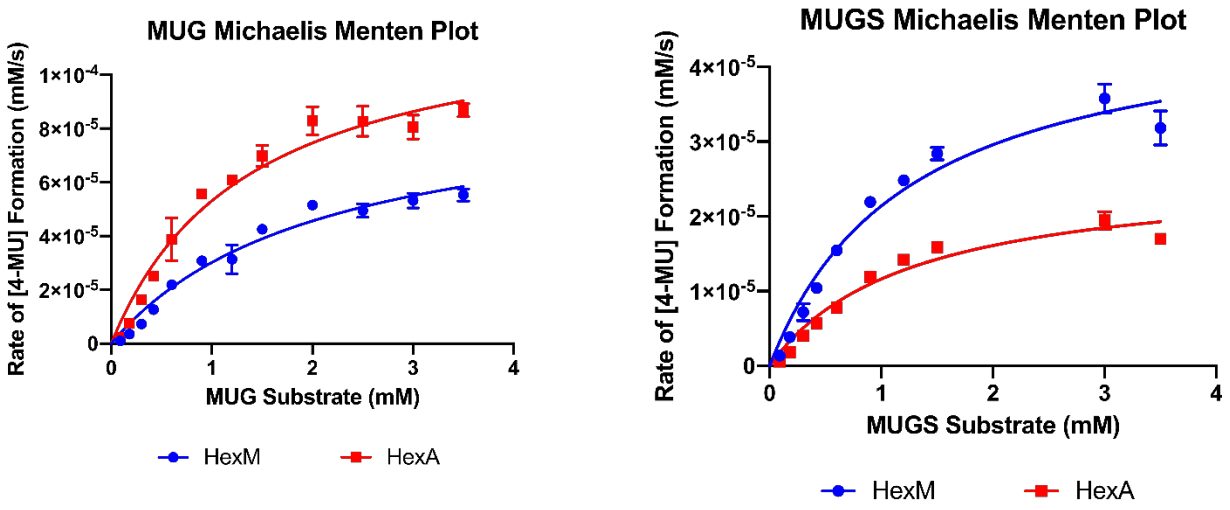

Figure 10: MUGS activity assay. Hydrolysis of negatively charged MUGS by HexA and HexM produced fluorescence that was detected using a SpectraMax iD5 plate reader measured as relative fluorescent units (RFU). Purified HexA was provided by Kristen Bouma. MUGS substrate and purified enzyme samples were diluted from stock concentrations in CP buffer (pH 4.2) supplemented with 0.5% BSA. Working enzyme concentration was 100pM. Rate of fluorescent product formation was calculated using a previously established method (58) . V_{max}, K_M and K_{cat} values were calculated using Prism8 (See Table 6).

Table 6: HexA and HexM kinetic values for MUG and MUGS substrates

	HexA MUG	HexM MUG	HexA MUGS	HexM MUGS
K_M (mM)	**1.365 ± 0.168**	**2.096 ± 0.312**	**1.252 ± 0.173**	**1.242 ± 0.152**
V_{max} (mM/s)	**$1.25e^{-4}$ ± $6.74e^{-6}$**	**$9.34e^{-5}$ ± $7.23e^{-6}$**	**$2.62e^{-5}$ ± $1.6e^{-6}$**	**4.79e-5 ± $2.58e^{-6}$**
K_{cat} (s^{-1})	**627.7 ± 33.72**	**467.0 ± 36.15**	**130.9 ± 8.00**	**239.7 ± 12.94**

The kinetic results for HexA were consistent with previously conducted MUGS assays ([24,42,58]). A MUG/MUGS hydrolysis ratio was also used to characterize the substrate specificity of the α- and β- subunits that form HexA ([58]). The β-subunit of HexA lacks the positively charged binding site of the α-subunit, and preferentially hydrolyzes the neutral substrate MUG. This explains the MUG/MUGS ratio of HexB (ββ) of 300:1, as compared to MUG/MUGS ratio of HexA (αβ) of 4:1 and of HexS (αα) (1:1) (24,58). The MUG/MUGS ratio established from our biochemical analysis was 4.8/1 for HexA and 1.9/1 for HexM. This result confirmed that the HexA (αβ) activity being produced was consistent with previously conducted experiments, and that HexM (μμ) maintained a relatively poor affinity for neutral substrates, as expected.

3.1.3 Long Term Stability Experiment

A MUGS assay was conducted on samples of HexM and HexA in phosphate buffer at pH 5.5 or pH 7 (See Figure 11). HexA and HexM were diluted in phosphate buffer (pH 5.5 or pH 7) to 1 nM and stored at 37°C in an incubator over the course of two weeks. HexM and HexA activity levels did not depreciate over the course of the experiment for either pH condition.

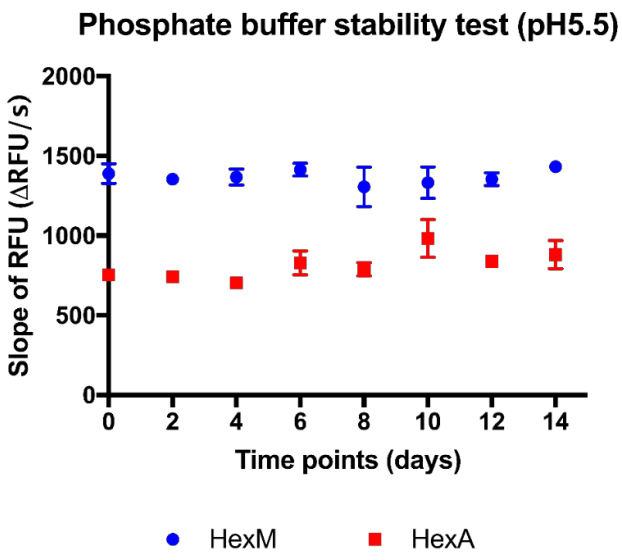

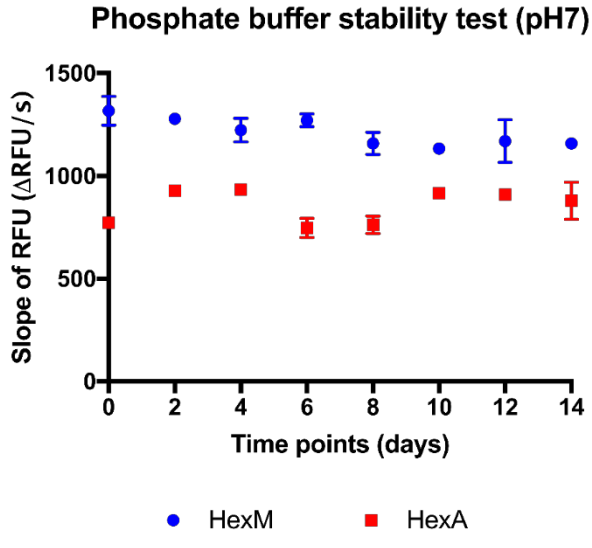

Figure 11: Long-term stability experiment. HexA and HexM were diluted in phosphate buffer (pH 5.5 or pH 7) to 1 nM and stored at 37ºC over the course of two weeks. Tubes were collected every 2 days and stored at -20ºC until the end of the experiment. Enzyme activity was analyzed by MUGS assay using 100pM of each protein, diluted in CP buffer supplemented with 0.5% BSA. Enzyme activity of each sample was assessed in triplicate by calculating the change in relative fluorescence units over the course of 30 minutes. Fluorescence produced by MUGS hydrolysis was detected using a SpectraMax ID5 plate reader. Error bars represent one standard deviation in each sample test. No significant difference was found in the MUGS activity levels of HexM or HexA over the course of the experiment (t-test $P > 0.05$)

The results of the long-term stability experiment were surprising, as it has been previously established that HexM is more thermally stable than HexA (42) and should therefore retain comparably more MUGS activity over an extended period. Future experiments assessing this may wish to vary the initial enzyme concentration used over the course of the incubation period.

3.2.0 Enhancing the cellular uptake of HexM

Cellular uptake experiments have previously shown that HexM is endocytosed and delivered to lysosomes and that this uptake can be reduced with the addition of free mannose-6-phosphate (M6P), implicating the M6P receptor pathway in its internalization (42,59). The enzymatic process of adding M6P to lysosomal enzymes to target them to the lysosome occurs in the Golgi network. (See Figure 12)

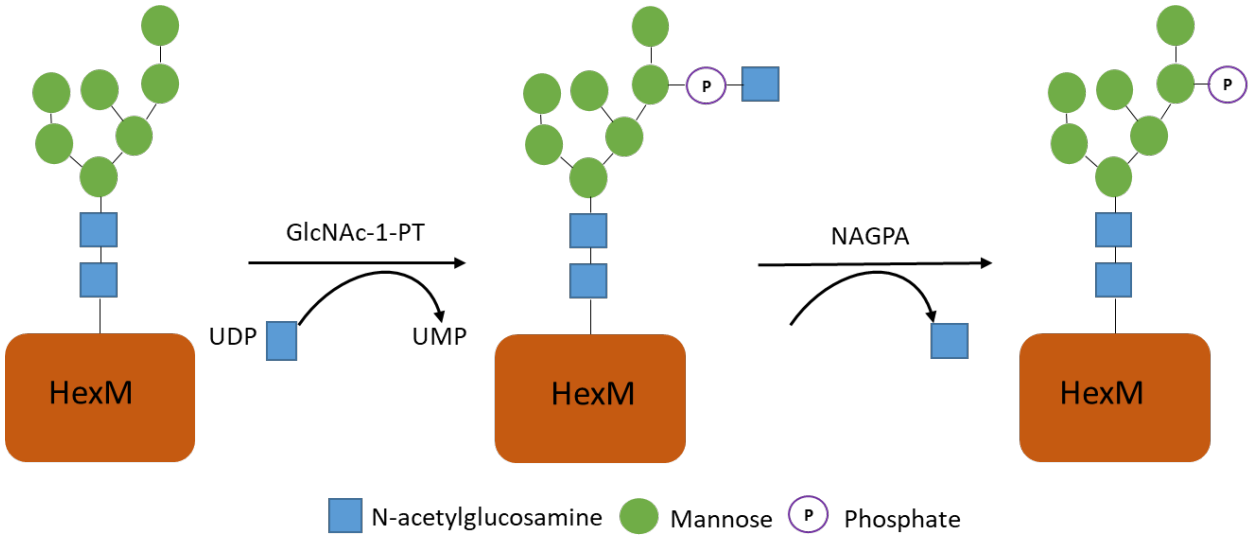

Figure 12: Diagram of GlcNAc-1-phosphotransferase function. Protein phosphorylation occurs in the Golgi apparatus where GlcNAc-1-PT facilitates the transfer of GlcNAc-attached phosphate to the mannose sugar residue of a glycosylated lysosomal enzyme. The GlcNAc residue is then cleaved by a N-acetylglucosamine-1-phosphodiester alpha-N-acetylglucosaminidase. M6P-tagged enzymes are bound by M6P receptors and delivered to pre-lysosomal compartments.

An issue regarding the large-scale production of recombinant enzyme necessary for ERT is inadequate *in cellulo* phosphorylation, due to endogenous levels of glycosylating and phosphorylating enzymes being incommensurate with the artificially increased production of recombinant enzyme in mammalian cells for treatment. Co-expression of recombinant proteins used in ERT (*i.e.* β-glucocerebrosidase and lysosomal α-glucosidase) with an engineered phosphotransferase has been shown to increase protein phosphorylation and cellular uptake in HeLa cells (48). To explore the potential therapeutic enhancement of increased HexM phosphorylation on uptake into Tay-Sachs disease fibroblast cells, HexM-producing cells were

co-transfected with pcDNA6/V5-His-GlcNAc-1-PT and assessed by cellular uptake assay. The initial results obtained from the assay lead to the construction of pcDNA6/V5-GlcNAc-1-PT-NoHis. There was concern that the results of the assay were a result of the co-purification of His-tagged GlcNAc-1-PT and HexM, which was resolved by removal of the His-tag from the pcDNA6/V5-GlcNAc-1-PT plasmid. Hyperphosphorylated HexM (phosHexM) was found to have improved cellular uptake compared to HexM, highlighting the therapeutic benefits of increased phosphorylation of recombinant enzymes. Furthermore, Matrix-assisted laser desorption/ionization mass spectrometry (MALDI-MS) analysis verified the presence of N-linked glycoforms containing mannose in samples of HexA, HexM and phosHexM. The goal of the MALDI-MS analysis was to assess relative phosphorylation levels between HexM and phosHexM. Though phosphates associated with N-linked mannose residues on phosHexM were detected, it was not possible to compare the phosphorylation of HexM and phosHexM. The results of these efforts are described below.

3.2.1 Production of GlcNAc-1-PT-NoHis

pcDNA6/V5-His-GlcNAc-1-PT was modified by removing the His-tag through site-directed mutagenesis to prevent its co-purification of GlcNAc-1-PT during the purification protocol of HexM. In collaboration with Steven Cooper, a summer student in Dr. Barbara Triggs-Raine's lab, activity assays assessing the cellular uptake of HexM into TSD fibroblast cells were conducted. Results of activity assays from TSD cellular uptake assays conducted with the His-tagged Glc-NAc-1-PT plasmid found a similar amount of MUGS activity in the cell lysates of HexM and phosHexM conditions. Enzyme activity from the cell media of both conditions were notably different, with cell media from the HexM condition having significantly higher MUGS activity. This result was counterintuitive, as the amount of exogenous HexM and

phosHexM provided to each well was the same. SDS PAGE of the proteins did not reveal any noticeable impurities, though further analysis revealed that the purified form of GlcNAc-1-PT (~65 kDa) possessed a similar size as denatured HexM (62 kDa). As the purification process of HexM involves using Ni-NTA resin to bind onto the His-tagged HexM, it was hypothesized that removal of the His-tag from the GlcNAc-1-PT plasmid would prevent expressed GlcNAc-1-PT from being purified with phosHexM. Site-directed mutagenesis was conducted on pcDNA6/V5-His-GlcNAc-1-PT with PCR primers specifically designed to remove the His-tag. The resulting GlcNAc-1-PT-NoHis plasmid was assessed by agarose gel, purified by gel extraction kit, and confirmed by sequencing (See Figure 13)

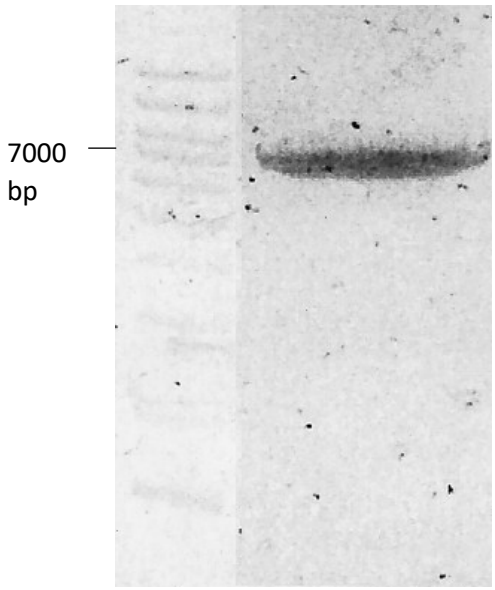

Figure 13: PCR amplification of pcDNA6/V5-His-GlcNAc-1-PT plasmid. The gel was visualized using a Gel Documentation System (Axygen, Corning, Life Sciences). Lane 1 contains 25 µl of the Dpn1-treated PCR reaction of Glc-NAc-1-PT plasmid (6805 bp). A 1 Kb Plus ladder was used to visualize bands. The gel fragment containing the plasmid was excised and processed using a QIAquick Gel Extraction Kit (Qiagen; Cat# 28115). The resulting cut

plasmid product (47 ng/µl) was assessed via NanoDrop and found to have an A260/280 of 1.9 and an A260/230 of 2.03.

Once GlcNAc-1-PT-NoHis was used in production of phosHexM for the cellular uptake study, the results more closely matched that of studies showing the effects of increased phosphorylation on lysosomal enzymes (41). Interestingly, the modified GlcNAc-1-PT had been found to localize in the Golgi, and therefore should not have been expressed in the media of the cotransfected HexABKOHexM HEK293T cell line (48). This may be due to the engineered GlcNAc-1-PT plasmid having 3- to 4-fold expression compared to wildtype GlcNAc-1-PT.

3.2.2 Co-Transfection of HexM and GlcNAc-1-PT-NoHis

Following the creation of GlcNAc-1-PT-NoHis, the plasmid was transfected into a HexM-producing HEK293T cell line. The resulting purified protein from the transfected cell line was compared to protein purified from non-transfected HexM-producing HEK293T cells. SDS PAGE and a western blot of the purified proteins confirmed the presence of HexM in both (See Figure 14). The degree of phosphorylation of the proteins was assessed via Phospho-Tag Phosphoprotein Gel Stain (ABP Biosciences, P005A), a highly sensitive fluorescent poly acrylamide gel stain designed for selectively complexing its zinc center with phosphate groups attached to phosphorylated amino acid residues (See Figure 15).

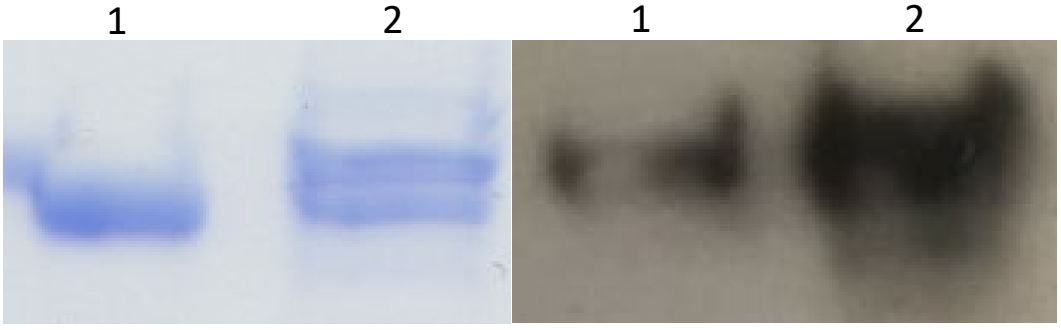

Figure 14: SDS PAGE and Western Blot of HexM and phosHexM. HexM-producing HEK293T cells were transiently transfected with GlcNAc-1-PT-NoHis. Media from control (Lane 1) and transfected cells (Lane 2) was collected and purified via IMAC and SEC. Protein sample concentrations were 1.5 mg/ml. 30 µl (~45 µg) protein was loaded into each well. Gel bands were observed at ~68 kDa. anti-HEXA antibody was used for western blot.

2

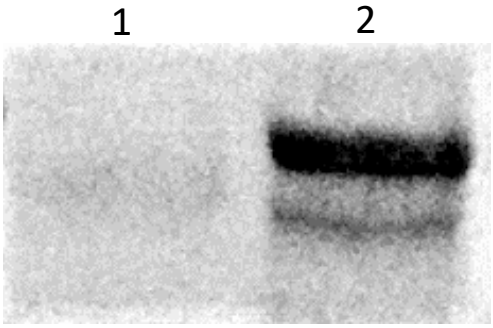

Figure 15: PhosphoProtein Gel Stain image. SDS PAGE gel was stained with Phospho-Tag. Lane 1 is purified HexM. Lane 2 is purified HexM transiently transfected with GlcNAc-1-PT-NoHis. Gel was visualized by UV illuminator.

3.2.3 Cellular Uptake assay comparing PhosHexM and HexM

Immortalized Tay-Sachs disease (TSD) fibroblast 1881 cells were used to test the cellular uptake of HexM and its highly phosphorylated form, phosHexM. Endocytosis was measured via MUGS activity assay to determine the specific activity of HexM present in the cell lysate

samples (See Figure 16). PhosHexM was found to be present in approximately three times the amount to that of HexM.

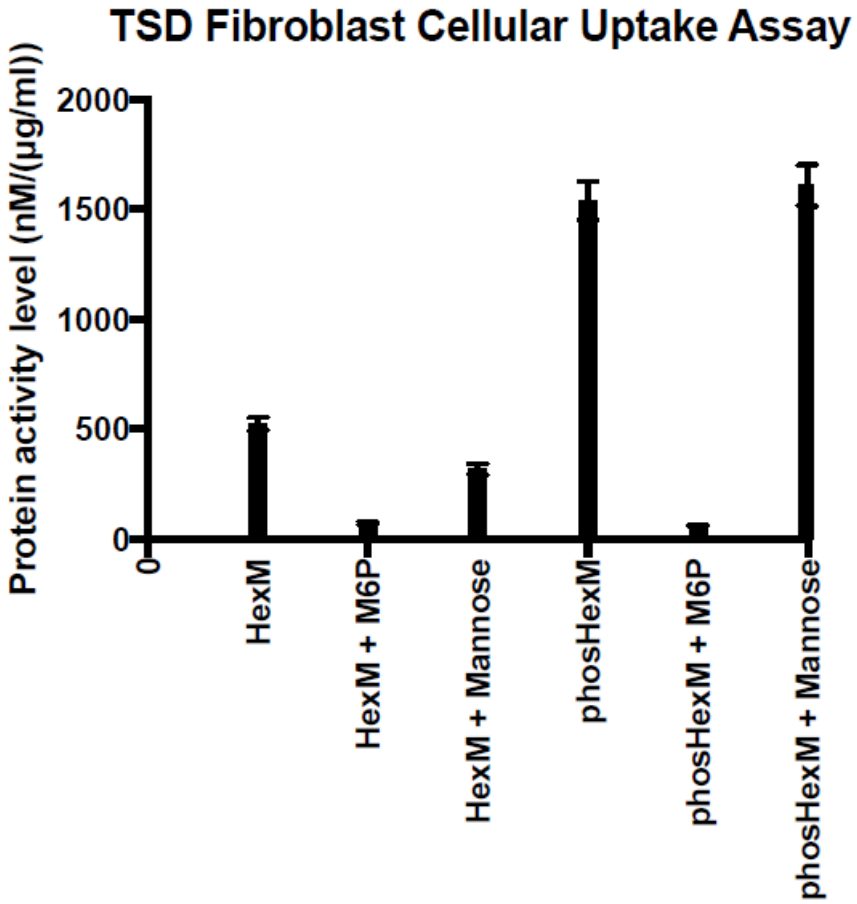

Figure 16: TSD Fibroblast cellular uptake assay. A modified GlcNAc-1-PT plasmid was co-transfected into a HexM-producing HEK293T cells to assess increased endocytosis into TSD fibroblast cells. Protein activity level is expressed as the ratio of the standardized MUGS activity versus the total protein concentration of each cell lysate sample. 15 µg of HexM or phosHexM was added to a 6 well plate containing TSD fibroblast cells. The final concentration of M6P or mannose present in the labelled conditions was 5mM. Cells were incubated with the protein, or the protein and added sugar, for 24 hours. Total protein concentration of cell lysates was

calculated by BSA standard assay. Protein specific activity was calculated by dividing the MUB concentration by total protein concentration for each sample, conducted in triplicate. Error bars represent one standard deviation in each sample test. phosHexM cell lysates samples had significantly more MUGS activity compared to HexM cell lysate (t-test $P < 0.005$, $R^2 = 0.99$)

This result suggests that recombinant HexM can be further phosphorylated to enhance its uptake into cells. Future clinical trials should employ intracranial injections to directly provide enzyme to affected tissue, as this method has been previously examined, and some of the main issues of enzyme replacement therapy methods could be addressed. Notably, there is a widespread distribution of neuronal cells that possess mannose-6-phosphate receptors present in throughout the CNS, highlighting the usefulness of the mannose-6-phosphate pathway in facilitating the delivery of exogenously provided HexM (60).

The increased risk of inflammation associated with intracranial injections of recombinant enzyme could also be reduced through further exploitation of the mannose-6-phosphate pathway. It has been found that HexA with a high M6P content produced from a modified *Ogatea minuta,* had an inhibitory effect on the production and induction of the chemokine MIP-1α in the hindbrains of intracranial injected SD mice (59). The inhibitory effect on macrophage inflammatory protein (MIP1-α) induction was greater than that of recombinant HexA with lower M6P content and significantly greater than the SD disease control mice. The authors reasoned that the increased cellular uptake of recombinant enzyme with high M6P content resulted in a reduction of enzyme circulating in the CNS, leading to a reduced inflammatory response. Disruption of the MIP1-α gene resulted in decreased microglial-associated neuroinflammation and neuronal apoptosis in a *Hexb* -/- SD mouse model (61). Therefore, increasing the M6P content of HexM could provide the solution to reducing neuroinflammation associated with the

intracranial administrations while simultaneously increasing the amount of enzyme that is taken up by affected neurons.

3.2.4 Mass Spectrometry Glycoform Analysis

Post-translational modifications are of critical importance to the production of functional HexA. The α and β- subunits of HexA are synthesized in the endoplasmic reticulum (ER), where they lose their signal peptide, form intra-chain disulfide bonds, and acquire N-linked oligosaccharides. These oligosaccharides are then phosphorylated by enzymes in the Golgi apparatus, to target the enzyme to lysosomes. Based on the amino acid sequence of HexM, glycosylation sites present on the α-subunit were expected to be present on the hybrid homodimer. Matrix-assisted laser desorption/ionization (MALDI) Mass spectrometry (MS) analysis, performed by Tyler Tran from Dr. Helene Perrault's lab (Chemistry, University of Manitoba), compared the presence of glycoforms and the phosphorylation level of HexA, HexM, and hyper-phosphorylated HexM (See Figure 17). The phosphorylation level of phosHexM was found to be higher than that of HexM, confirming the increased phosphorylating ability of the GlcNAc-1-PT-NoHis used to produce phosHexM.

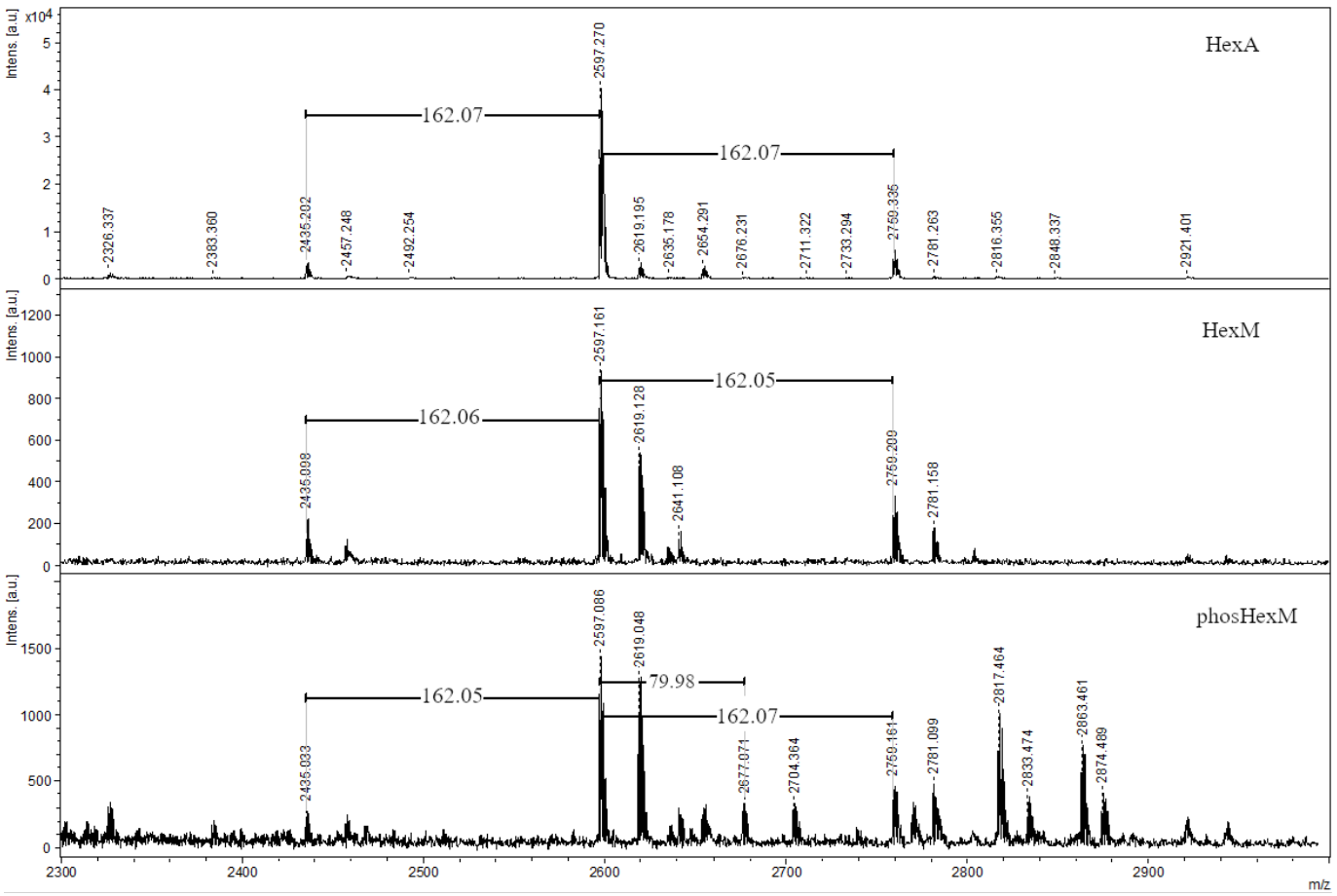

Figure 17: MALDI-MS analysis of HexA, HexM, and phosHexM. Matrix-assisted laser desorption/ionization (MALDI) Mass spectrometry (MS) analysis was performed by Taylor Battelino from Dr. Helene Perrault's lab (Chemistry, University of Manitoba) as previously described (See Methods). Each sample was digested with Endoproteinase GluC in order to assess the N-linked glycosylation region (GTFFINKTE). Mannose residues (Δm/z = ~162.05) are shown, indicating the presence of multiple glycoforms in each sample. The presence of phosphate (Δm/z = 79.96) was noted in the phosHexM sample.

3.3.0 Structural Studies of HexM

Although the three-dimensional crystal structures of HexA and HexB are known and were used to guide the design of HexM, the crystal structure of HexM itself has not been determined, nor has a crystal structure of HexA or HexM been determined bound to GM2AP to understand how these proteins interact. How they interact has only been predicted from computer modeling. To fully understand the molecular basis for the remarkable enzymatic activity of HexM, I attempted to carry out a combination of molecular and structural biology methods to determine the 3D crystal structure of HexM alone and bound to GM2AP. The goal of the work was to determine precisely how HexM interacts with GM2AP to inform further engineering of the biochemical properties of HexM for its potential use as a biopharmaceutical to treat G_{M2} gangliosidosis. While I was able to determine the X-ray structure of HexM, which provides excellent insight in the HexM function, I was unable to devise conditions to capture HexM bound to GM2AP for subsequent structural work. The results of these efforts are described below.

3.3.1 X-ray crystallographic structural analysis of HexM

Purified recombinant HexM (10 mg/ml) from a HexM-producing HEK293T cell line was crystallized. HexM crystallized in space group $P2_1$ with two HexM homodimers (1964 residues) in the asymmetric unit. An initial phase estimate was determined by molecular replacement, using the previously solved structure of HexA (PDB ID: 2GK1) as the search model. The structure of HexM was solved at a resolution of 2.8 Å and refined to a R_{work} of 0.27 and a R_{free} of 0.32 (See Table 7)**.**

Table 7. Crystallographic Statistics Table

X-ray diffraction data and atomic refinement of HexM

Crystal geometry	
Space group	$P2_1$
Unit cell dimensions (Å)	*a* = 78.98 *b* = 88.707 *c* = 165.809; β = 90.055°
Crystallographic data	
Wavelength	1.5418
Resolution range (Å)	46.91 - 2.809 (2.909 - 2.809)[α]
Total observations	207686
Unique reflections	55758 (5273)
Multiplicity	3.7
Completeness (%)	99.22 (94.41)
R_{merge}	0.163
$CC_{1/2}$	0.987
I/σ(I)	6.5
Wilson B-factor (Å²)	52.3
Refinement statistics	
Reflections in test set	1994
Protein atoms	31574
Solvent molecules	141
R_{work} (R_{free})	0.27 (0.32)
Root mean square deviations	
Bond lengths/angles (Å / °)	0.007/1.25
Ramachandran plot	
Favored/allowed (%)	92/8
Average B-factor (Å²)	55.88
B-factor for macromolecules	56.01
B-factor for solvent	41.59

[α] Values in parentheses refer to the highest resolution shell.

3.3.2 HexM Active Site

The HexM μ-subunit was engineered to contain the α-subunit active site, regions of the surfaces of the α and the β subunits necessary for GM2:GM2AP interaction, and the β subunit interface needed to form a stable homodimer (42). Analysis of the structure revealed that two identical μ-subunits that interact to form a homodimer similarly to HexA and HexB, as expected**.** The position of μAsp321 and μGlu322 in each μ-subunit active site matches that of corresponding residues (αAsp322 and αGlu323) in the α-subunit active site of HexA (See Figure 18), providing further evidence that HexM possesses two alpha subunit active sites.

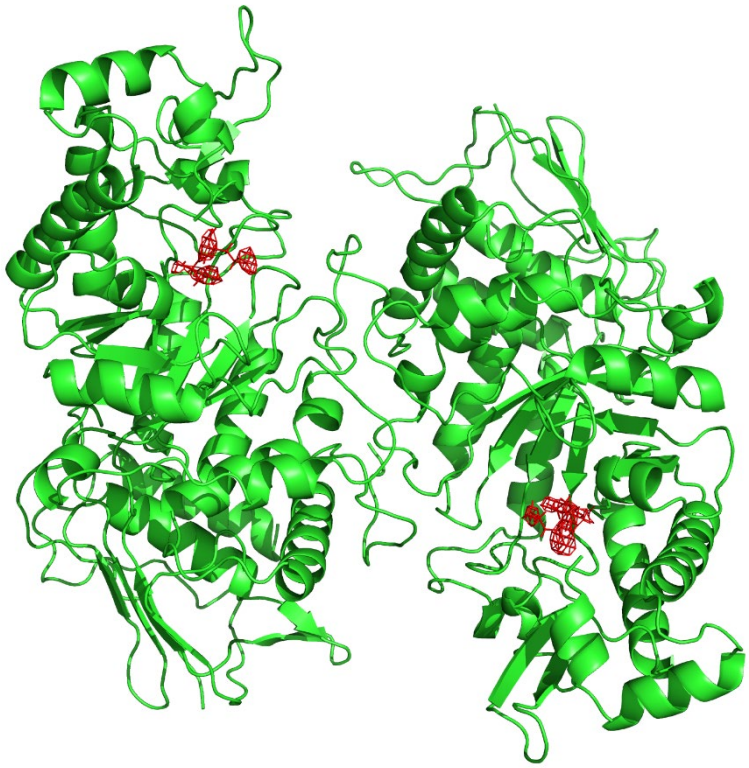

Figure 18: Ribbon diagram of HexM active sites. The μ subunit is a modified α-subunit that has retained the enzyme's active site. The active site residues Glu322 and Asp321 (in red) are shown for both μ subunits (green). The electron density (mesh) of the active site is shown. Images were taken in PyMOL (62).

3.3.3 Structural analysis of HexM β-subunit interface

The substitution of the stable β-subunit dimerization interface into each μ-subunit increased the melting temperature (Tm) of HexM (62ºC) in comparison to HexA (53ºC) (42). Indeed, the substituted amino acids from the β-subunit were present in the μ-subunit dimerization interface forming a beta/beta dimer interface as seen in HexB, as predicted from the HexM design strategy (See Figure 19).

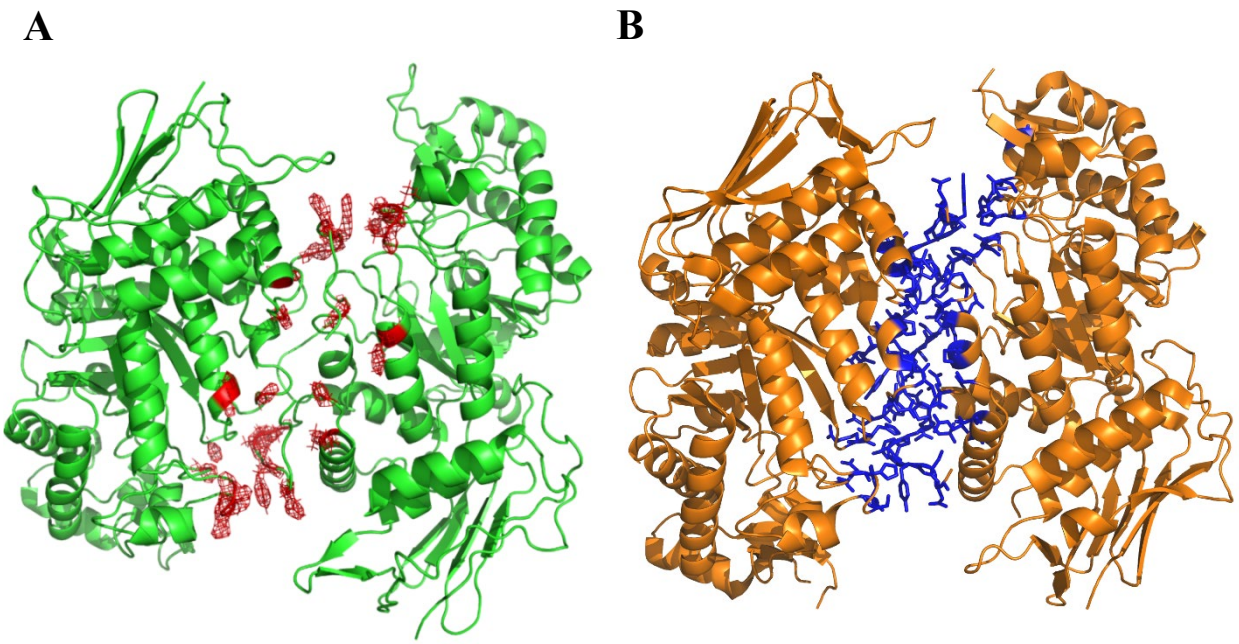

Figure 19: Orientation of HexM dimer interface. Amino acids from the β subunit of HexA were substituted in the μ subunit to produce a stable β subunit–like interface. A. The stable β subunit interface (in red) present between the two μ subunits (in green) of HexM are shown. The electron density (mesh) of the substituted amino acids is also shown. B. The amino acids (in blue) of the beta/beta dimer interface present between the two β subunits (in orange) of HexB are shown.

3.3.4 Orientation of HexM monomers

It has been previously suggested, based on predictive modelling, that HexM could bind a GM2-GM2AP complex at each of its two active sites without significant steric hindrance. Based on the crystal structure of HexM, the monomeric μ-subunits appear to be dimerized in an antiparallel-like orientation (See Figure 20). This would allow GM2-GM2AP complexes to bind in a *trans* manner across both GM2AP binding regions present on the protein surface.

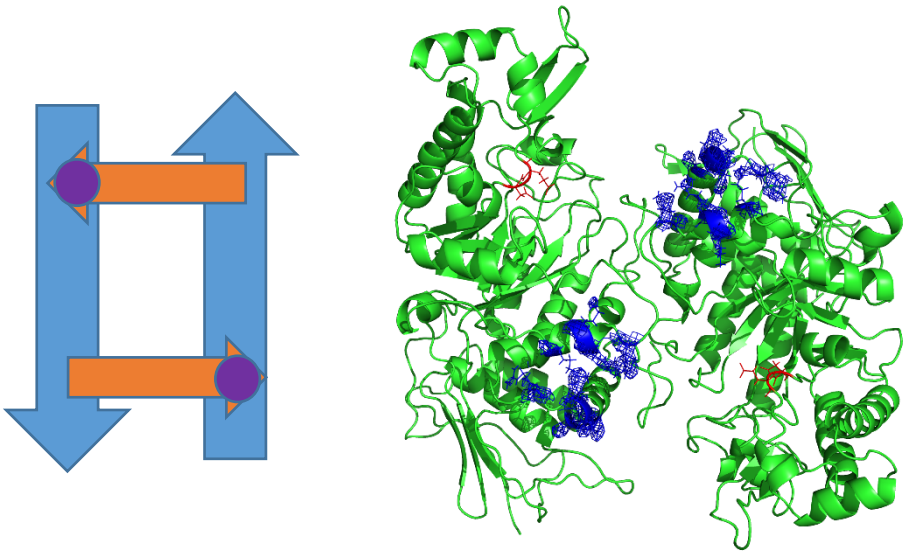

Figure 20. Orientation of HexM monomers. HexM monomers (blue arrows) are oriented in an antiparallel-like manner. GM2AP (orange arrows) carrying a GM2 ganglioside (purple circle) orients itself in *trans* to present the substrate to the active site of HexM. A structural image of HexM is shown on the right, with the GM2AP binding regions (blue) and GM2 ganglioside active site (red) being highlighted.

Interestingly, the *trans* positioning of GM2AP and GM2 ganglioside is how the α-subunit and β-subunit of HexA interact with the same molecules, indicating that the binding interaction was preserved in the modifications made to create the μ-subunit (63). The availability of the GM2AP binding sites and positioning of the active sites confirms that the increased binding

capacity of HexM is due to the modifications made to the μ-subunits, allowing for them to dimerize and retain functionality. As HexM has double the capacity to bind and process GM2 ganglioside, less, if not half, of the total enzyme would be necessary to administer to patients via injection to reach the critical threshold of 10% normal HexA functionality (Figure 21).

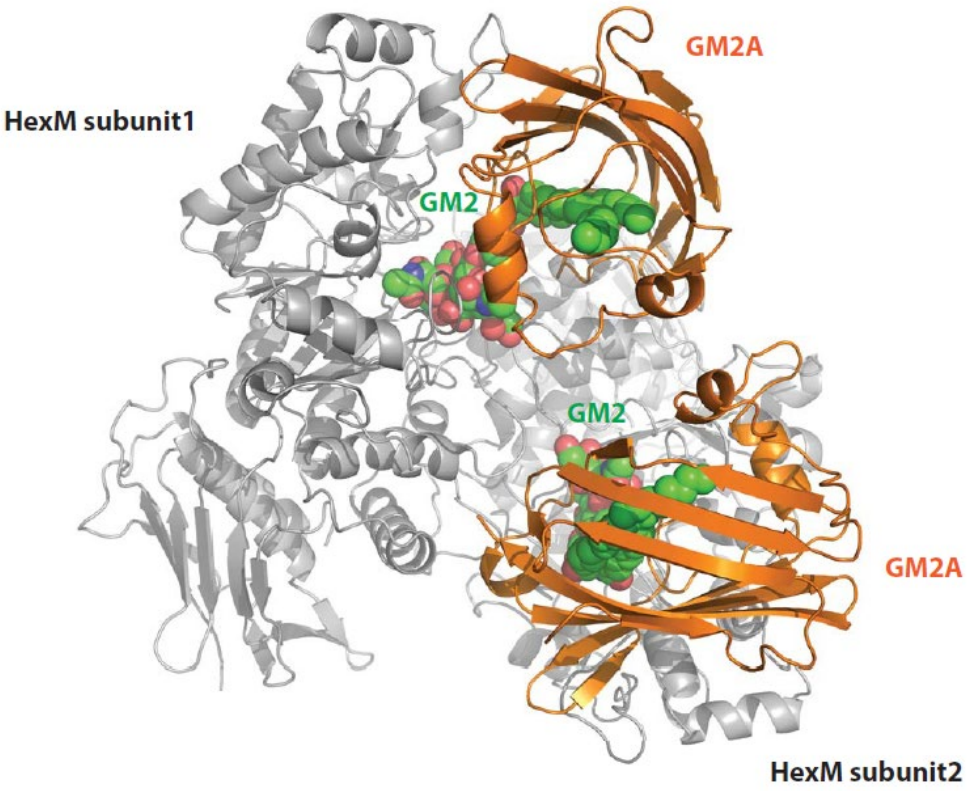

Figure 21: Model of HexM homodimer bound to complexes of GM2A/GM2. The model shows the positioning of GM2 activator protein (GM2A, in orange) bound with GM2 (GM2 ganglioside, in green) complexed with each individual μ-subunit of HexM (shown in gray).

3.4.0 Complexing HexM with GM2AP to gain insight into GM2 turnover

Experimentally determined structures of GM2AP bound to HexM or wild type HexA are not available. How these proteins interact has only been predicted from molecular modelling, which is prone to error (5). Thus, to truly understand how HexM recognizes and binds GM2AP

with GM2 ganglioside, I first inactivated the catalytic activity of HexM by mutating the active site glutamic acid 322 to glutamine. Given the glycolytic mechanism of HexM, we expected the Glu322Gln mutation to cause HexM to bind the GM2AP:GM2 complex as a long-lived enzyme-substrate complex that would be unable to turnover GM2 to GM3. Glu323 does not participate in substrate binding. However, it is required to cleave a covalent bond in GM2, which, once broken, causes the complex to dissociate. The following section describes my attempts to generate a stable HexM (Glu322Gln):GM2AP complex. Although I was not successful, I established some steps needed to ultimately generate this complex for future structural investigations.

3.4.1 HexME322Q Activity Assessment

To understand the molecular basis for how HexM interacts with GM2AP to turnover GM2 ganglioside, I first inactivated the glycolytic activity of HexM by mutating the general acid-base residue Glu322 (See Fig 22) to the non-ionizable glutamine, preventing the ability of HexM to turnover substrate.

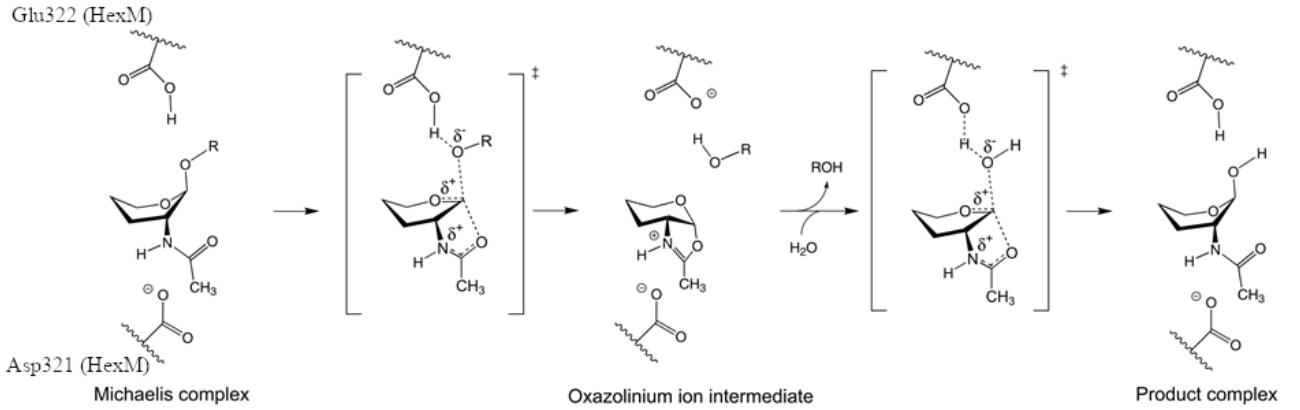

Figure 22: The proposed catalytic mechanism for HexM. The Asp 321 and Glu 323 residues are shown. Asp 321 is involved in orienting the C2-acetamido group of GM2 ganglioside into position for nucleophilic attack and subsequently stabilizing the positive charge on the oxazolinium ion intermediate. Glu323 acts as a general acid-base residue, facilitating the cleavage of the GalNAc sugar from GM2 ganglioside. The image has been modified from its original source (5). Reproduced with permission of Oxford University Press via Copyright Clearance Center.

We hypothesized that this mutation would enable HexM to capture the GlcNAc reside of GM2 (bound within GM2AP) but not cleave it off, thereby generating a stable complex for crystallization trials. A single amino acid substitution, Glu322Gln (E322Q), was generated in the PB-T-RfA-HexM construct by PCR amplifying an 861 bp synthetic double stranded DNA (gBlock) encompassing a section of the HexM insert and the E322Q mutation (See Fig 23).

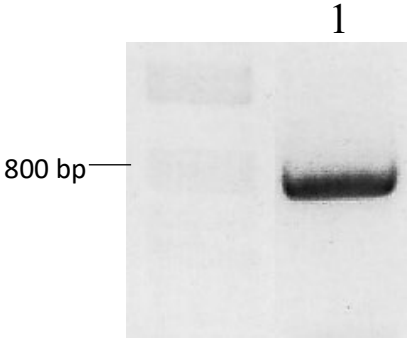

Figure 23: PCR amplification of gBlock. The synthesized gBlock, consisting of an 861 bp portion of HexM cDNA with an amino acid substitution E322Q, double-stranded DNA fragment (Integrated DNA Technologies). To assess the band size, a 1 Kb Plus DNA ladder (Invitrogen, ThermoFisher Scientific), labelled on the right, was used. 25µl of the PCR product was added (Lane 1). The purified gBlock (134.8 ng/µl) was assessed via NanoDrop and found to have an A260/A280 of 1.83 and an A260/A2340 of 2.14. The gBlock was then double digested using

restriction enzymes AflII and AfeI, then purified with using Qiaquick PCR Purification Kit (Qiagen; 28104). The resulting purified double-digested gBlock (87.2 ng/µl) was assessed via NanoDrop and found to have an A260/A280 of 1.86 and a A260/A230 of 2.05.

The PB-T-RfA-HexM (~8000 bp) construct was also double-digested using the enzymes AflII and AfeI (See Fig 24)

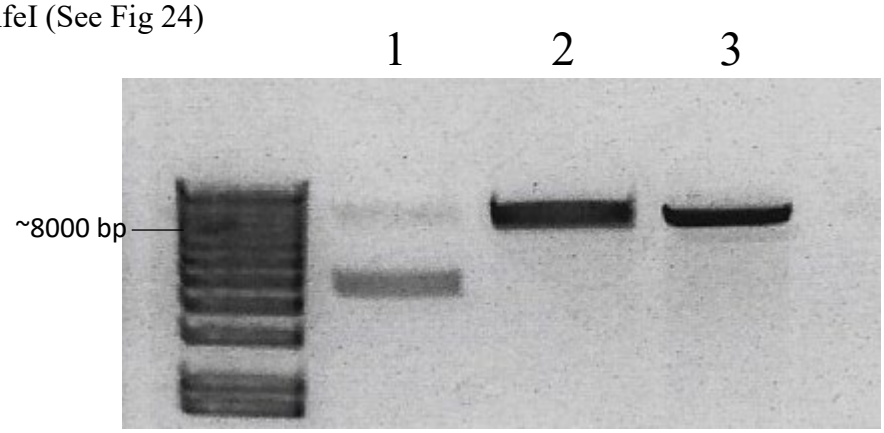

Figure 24: Enzyme restriction digest of PB-T-RfAHexM plasmid. Restriction enzymes used were AflII and AfeI. All reactions contained 2.5 ng plasmid DNA. Lane 1 is supercoiled PB-T-RfAHexM plasmid (5 Kbp). Lane 2 is AflII-digested plasmid (~8 Kbp). Lane 3 is AflII and AfeI double digest of the plasmid (~7.5 Kbp). A 1 Kb Plus ladder was used to visualize bands.

Following the double digest, the plasmid was loaded in excess into an agarose gel and extracted for subsequent purification. A gel extraction kit (Qiagen; 28115) was used to clean up the extracted gel fragment. The resulting cut plasmid product (98.9 ng/µl) was assessed using a NanoDrop One (ThermoScientific) and found to have an A260/280 of 1.87 and an A260/230 of 2.07.

The double digested PB-T-RfA plasmid and gBlock were ligated together with Instant Sticky-End Ligase Master Mix (NEB, M0370L), and transformed into competent dH5α *E. coli* (NEB). A negative control of *E. coli* with dH_2O was also produced. Colonies were found on the

vector with insert plate, while none were found on the negative or vector control plates. In order to determine the most effective transformation, a colony PCR was conducted on 7 selected colonies using the same PCR parameters and primers as used in the amplification of the gBlock. The resulting PCR products were visualized on an 1.2% agarose gel (See Fig 25).

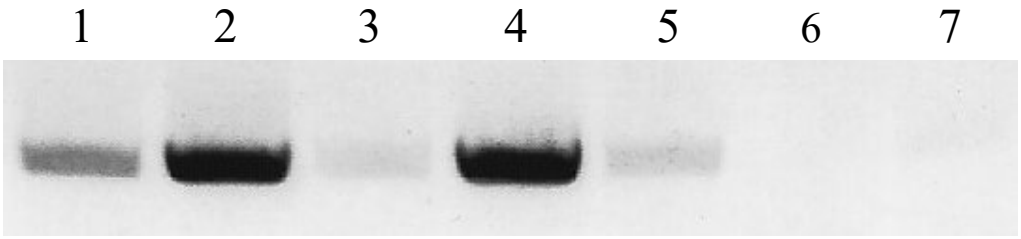

Figure 25: Colony PCR results. Transformed *E. coli* colonies were heat lyzed and PCR amplified with the same thermocycling condition and primers used to amplify the gBlock. Seven colonies were assessed in this way, labelled above. All bands were present at ~794 bp. The colonies in lanes 2 and 4 were selected for further analysis.

A QIAprep Spin Miniprep Kit was used to isolate purified plasmid from the transformed *E. coli* and the resulting products were assessed by NanoDrop. The plasmid from colony 2 (541.3 ng/µl) had an A260/A280 of 1.91 and an A260/A230 of 2.26. The plasmid from colony 4 (547.9 ng/µl) had an A260/A280 of 1.91 and an A260/A230 of 2.29.

The PB-T-RfA-HEXME322Q plasmid purified from colony 2 was transfected into HexABKO HEK293T cells using a Gateway *piggyBac* transposon expression system, previously used to transfect HEXM into HexABKO HEK293T cells (See Materials and Methods). Media was collected from the transfected HexABKOHexME322Q HEK293T cells grown in T-75 flasks. HexME322Q was purified from pooled flask media via immobilized metal affinity

chromatography (IMAC) and size exclusion chromatography (SEC). Protein expression of HexME322Q was confirmed by western blot (ab91624; Abcam) (See Fig 26).

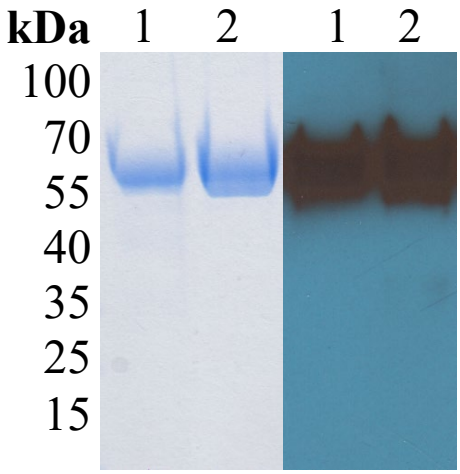

Figure 26: SDS PAGE gel and Western Blot of HexM and HexME322Q mutant. SDS PAGE protein sample concentration was 1 mg/ml. Western blot sample concentrations were diluted to 50 µg/ml. Lane 1 is purified HexME322Q Lane 2 is purified HexM. Bands of both samples were observed at ~65 kDa.

HexM and HexME322Q activity levels were compared via a MUGS activity assay (See Figure 27). There was little difference in activity levels between the CP buffer blank and HexME322Q in the presence of 600 µM MUGS. Thus, the E322Q mutation successfully removed the glycolytic activity of HexM as expected and I now had the mutant form of the enzyme to attempt to complex with GM2AP loaded with GM2.

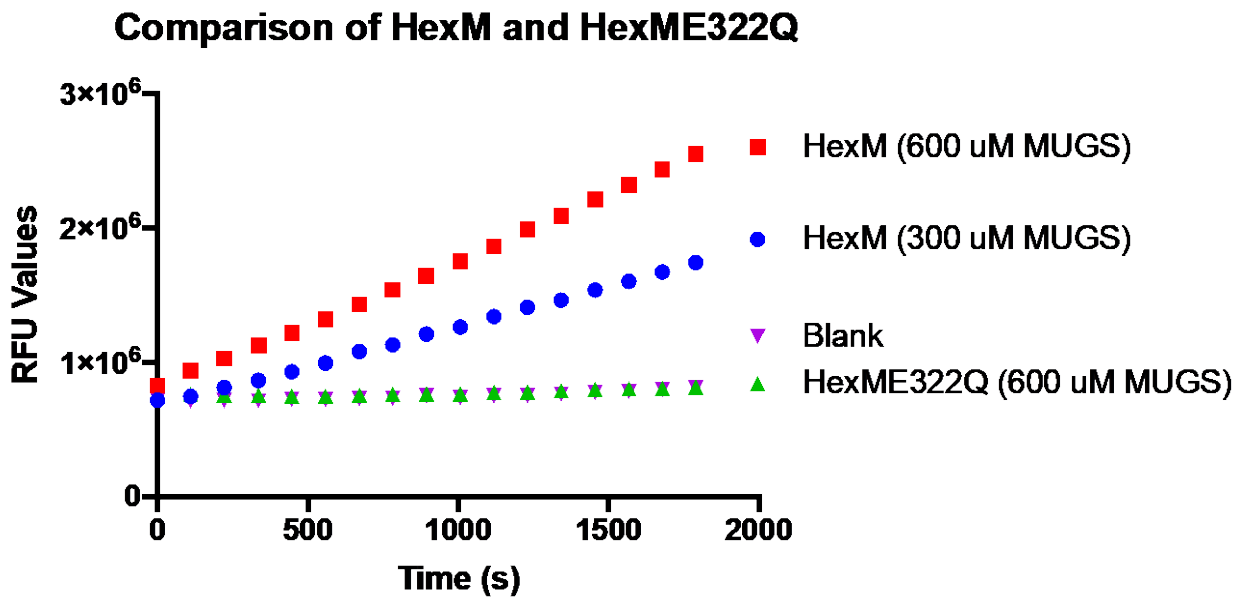

Figure 27. Activity assay comparing MUGS hydrolysis of HexM and HexME322Q. HexME322Q and HexM protein concentrations were 100 pM. MUGS concentration was stated in brackets. Protein samples were tested in triplicate and detected using a SpectraMax iD5 plate reader.

3.4.2 TEM Negative Stain Imaging

Negative stained images were imaged with a FEI Tecnai F20 TEM, operated at 200 kV by Daniel R. Beniac. In order to assess the general shape of specimen being assessed, an image of a small amount of protein was taken at 100,000x magnification. (See Figure 28)

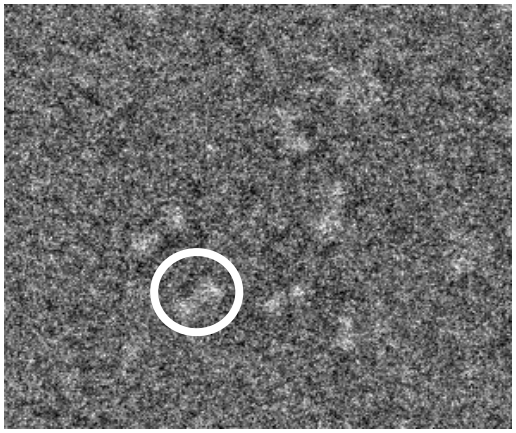

Figure 28: Negative stained specimen. Image was taken by transmission electron microscope (100,000x magnification). The dumbbell shape (white circle) is an example of a single observed specimen.

The shape of the specimen was further analyzed by compiling their images taken in different orientations (See Figure 29). Two distinct specimens are present in each image.

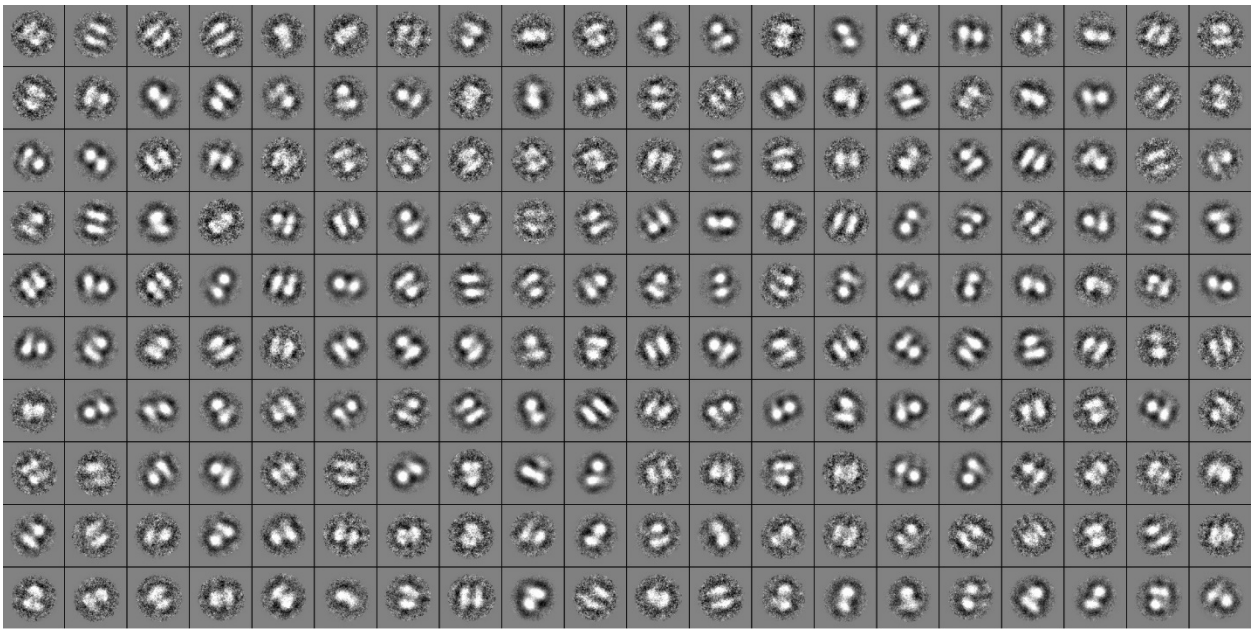

Figure 29. Compiled Transmission Electron Microscopy (TEM) images. HexM concentrated to 1.5mg/ml in phosphate buffered saline (PBS) (pH 7.0) was imaged via negative staining with a FEI Tecnai F20 TEM. Each image was taken at 100,000x magnification. The images were compiled by Dr. Daniel R. Beniac.

A 3-dimensional reconstruction of the hypothetical configuration of HexM was generated from the compiled 2D images (See Figure 30). Each μ-subunit (~68 kDa) can be seen in the reconstructed image. This method of visualizing protein may be used to assess binding capacity of GM2AP (~22 kDa) onto HexM, once a stable long-lived GM2-HexM complex can be created and purified.

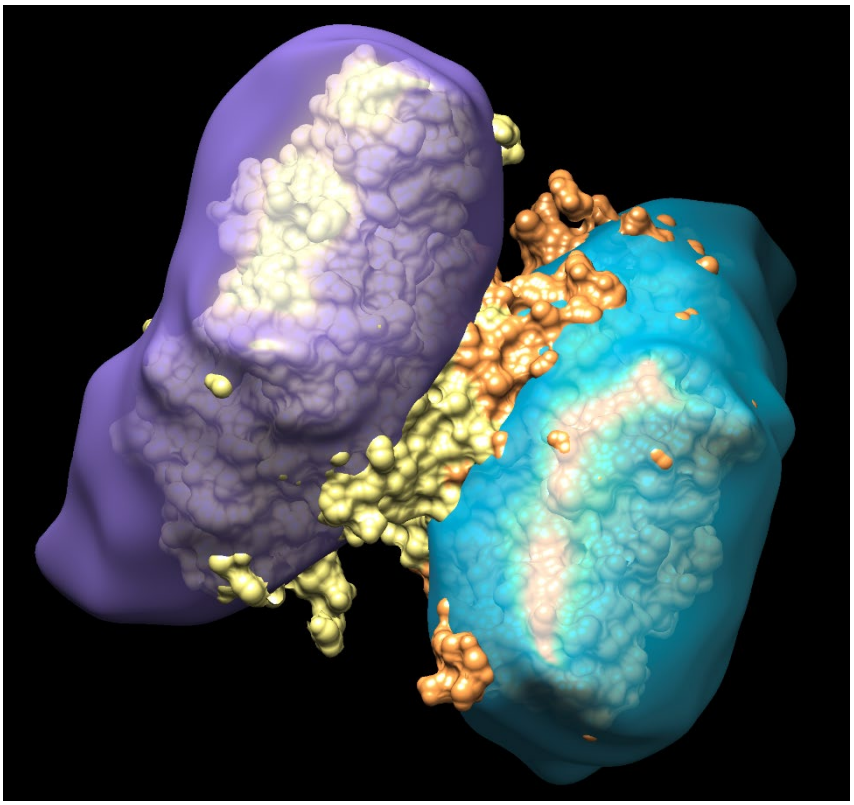

Figure 30: **Average EM envelope of the HexM dimer.** (Purple and cyan surfaces) fit onto the the X-ray structure of HexA (PDB:2GK1). Envelope calculated by Dr. Daniel Beniac, National Microbiology Laboratory. Image generated using UCSF Chimera (64)

3.4.3 Production of GM2AP

In order to assess the binding of HexM to GM2AP, it was necessary to produce GM2AP in enough quantities for analysis. Purified GM2AP was assessed via SDS PAGE and Western Blot (See Figure 31)

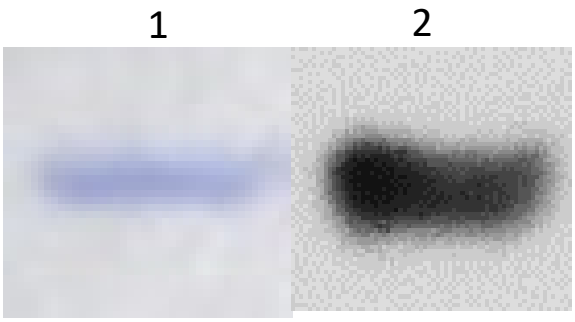

Figure 31: SDS PAGE and Western Blot of purified GM2AP. GM2AP (~22kDa) was collected from a HiLoad 16/600 Superdex 75 (GE Life Sciences) gel filtration column Protein was resolved in SDS-PAGE under reducing conditions (Lane 1), transferred to a nitrocellulose membrane, then detected with an anti-GM2AP Rb polyclonal antibody (ab224246, Abcam) using the manufacturer's protocol described (1/500 dilution) (Lane 2).

3.4.4 HexM-GM2AP Pulldown Assay

A pulldown assay modified from a study on the complex formation of galactosylceramidase and its coenzyme saposin-A was conducted to assess the presence of HexM-GM2AP complex formation (65). In order to facilitate the interaction between GM2AP and HexM, GM2-containing liposomes were formed and used to incubate purified GM2AP prior to binding studies. Based on predictive modelling, the GM2 ganglioside present in the liposomes could be necessary in the formation of a HexM-GM2AP complex.

GM2-containing liposomes that were produced were analyzed for size distribution via dynamic light scattering (See Figure 32)

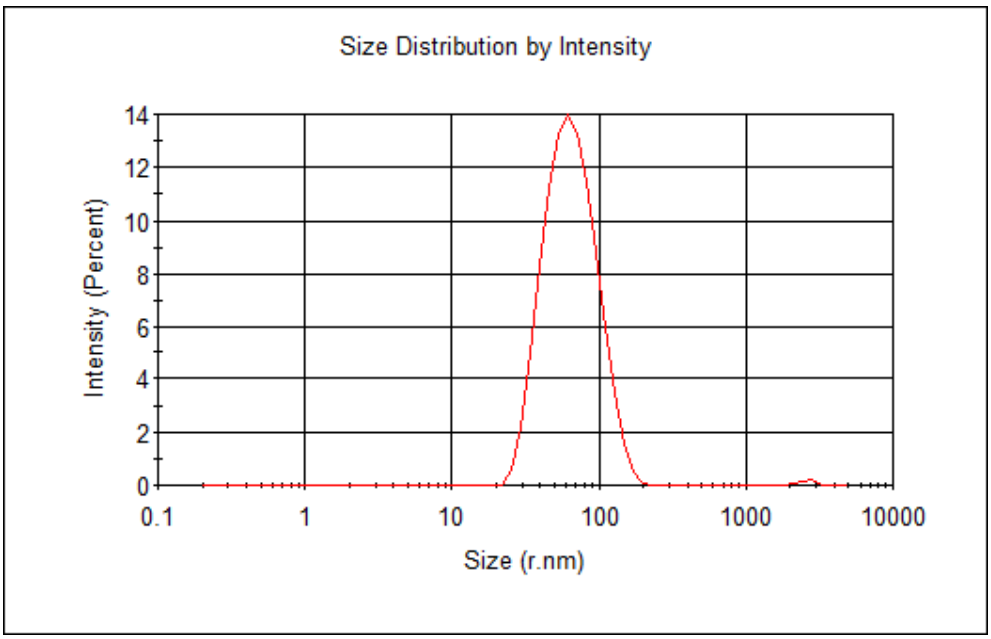

Figure 32: Averaged size distribution of 10 runs of 0.25mM liposome mixture. 40 µl of lipid sample was aliquoted into a disposable micro cuvette (Malvern Panalytical, ZEN0040) and analyzed with a Zetasizer Nano-S Dynamic Light Scattering (DLS) instrument (Refractive index: 1.45, Abs: 0.001). 15 measurements were taken per run.

The incubation of GM2AP with liposomes (containing GM2 or not containing GM2) was not found to influence GM2AP-HexM interaction and were therefore not explored further.

GM2AP was incubated in the presence of either CP buffer (pH 4.2) or sodium acetate buffer (pH 5.4) prior to being added to HexM-loaded magnetic Ni-NTA resin (See Figure 33). A faint band corresponding to the presence of GM2AP (~22kDa) in the elution step of the sodium acetate buffer is visible (Lane 2).

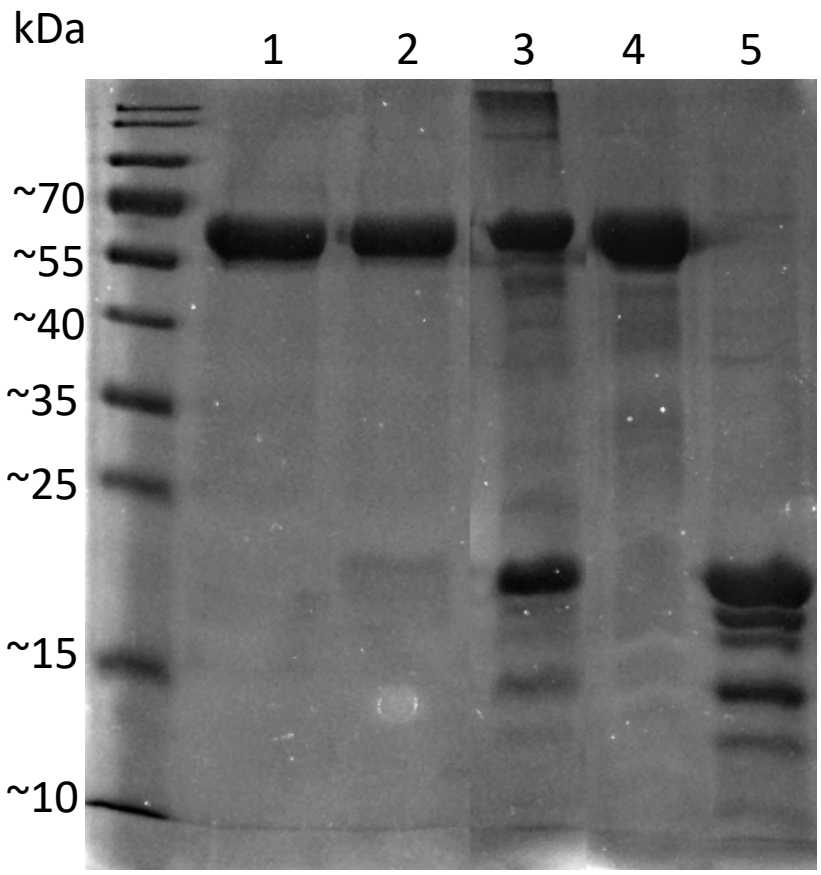

Figure 33. Pulldown assay of HexM-GM2AP. HexM was bound to magnetic Ni-NTA resin then combined with GM2AP varying pulldown buffers. HexM (30 µg) in 10mM Bis-Tris (pH 6.0), 100mM NaCl was applied to 50 µl magnetic Ni-NTA resin (Pierce). Concentrated GM2AP (~70 µg) in 5mM Tris (pH 7.0), 50mM NaCl. Pulldown buffers used varied, all contained v/v 0.05% Tween-20. Lane 1: Elution step of CP buffer condition (pH 4.2) Lane 2: Elution step of 100mM Sodium acetate condition (pH 5.4). The visible band is highlighted (white rectangle). Lane 3: First wash step post-GM2AP (from CP buffer). Lane 4: HexM control. Lane 5: GM2AP control.

Though there may be value in pursuing the GM2AP pulldown assay to bind GM2AP to HexM, the interactions assessed were relatively weak and subsequent pulldown assays were not explored further.

4.0 Conclusion and Future Directions

The creation of HexM has overcome many issues regarding the delivery of HexA by development of a μ-subunit capable of self-dimerizing with increased activity, substrate binding capacity, and thermal stability. This research further advances the use of HexM as an enzyme replacement therapy for GM2 gangliosidoses. HexM has been shown to be highly stable at 37ºC for at least two weeks and can be purified in gram-scale large quantities. In order to overcome the issue of inadequate *in cellulo* phosphorylation of recombinant enzyme production, co-transfections were conducted with the goal of improving phosphorylation. When co-transfected with an engineered GlcNAc-1-PT, HexM was adequately phosphorylated, as assessed by Phosphoprotein Phos-tag gel stain, and had a 3-fold increase in cellular uptake into TSD fibroblast cells. Further improvement in phosphorylating HexM may prove useful in increasing cellular uptake to an even greater extent. MALDI-MS analysis confirmed the presence of phosphate groups on mannosylated glycan residues of phosHexM, highlighting the usefulness in analytical chemical techniques to assess phosphorylation levels of recombinant enzymes.

A crystal structure of HexM, combined with mass spectrometry-based glycoform analysis, revealed how the engineering used to create the μ-subunit imparts stability and GM2AP binding to the HexM dimer, which retained proper folding and possessed N-linked mannosylated glycoforms in the same region as HexA. The amino acids substituted to create the dimer interface of HexM were in a similar position to the β-subunit dimer interface of HexB, indicating the modifications made to the μ-subunit improved thermal stability. Furthermore, the crystal

structure revealed that there is ample space for GM2AP, and presumably GM2 ganglioside, to bind concurrently to either binding region present on HexM.

In order to achieve sustained HexM-GM2AP complex formation, a HexME322Q mutant was produced. Abrogated MUGS cleavage activity of HexME322Q proved that Glu322 is a necessary amino acid in processing substrate at the active sites of HexM. Incubation of GM2AP with GM2-containing liposomes did not improve binding of GM2AP and HexM in pulldown assays. The use of HexME322Q in the pulldown assay also did not improve HexME322Q-GM2AP complex formation, though further experiments are needed to confirm this. Indeed, subsequent pulldown assays found that the buffer pH used to incubate GM2AP may play a role in facilitating HexM-GM2AP interaction. Future HexM-GM2AP complex studies may wish to explore additional buffer compositions to improve binding.

Studies demonstrating the potential of HexM in animal models still face limitations, including immunogenicity and impaired delivery through the blood-brain barrier (BBB)([66,67]). Structural analysis of surface antigens created as a result of genetic modification will improve our understanding of how HexM elicits an immune response. Furthermore, a promising approach to crossing the blood-brain involves fusing HexM to BBB shuttle tags, enabling receptor-mediated transcytosis of the enzyme into the central nervous system. The structure of HexM can be assessed to select areas for shuttle tag fusion without compromising enzyme stability or activity. The next steps in crystallization studies of HexM should involve solving the structure of the enzyme-coenzyme-substrate complex complexing of HexM-GM2AP-GM2 to further our understanding in how the recombinant protein interacts with GM2AP and processes GM2 ganglioside. Crystallographic analysis of the HexM-GM2AP-GM2 complex may prove too difficult, but my research also highlights the usefulness of transmission electron microscopy

imaging in providing structural insights of HexM. The presence of the two dimerized μ-subunits (~68 kDa) that constitute HexM were easily distinguishable and TEM images may have enough resolution to identify GM2AP (~22 kDa) bound to HexM, once sustained complex formation is achieved. Together, these studies will further the clinical potential HexM as a therapeutic to manage GM2 gangliosidoses.

Chapter 5: References

1. Sonnino, S, Mauri, L, Chigorno, V and Prinetti, A (2007). Gangliosides as components of lipid membrane domains. *Glycobiology* **17**: 1R-13R.

2. GRAVEL, RA (1995). The GM2 gangliosidoses. *Metab. Mol. basis Inherit. Dis.*: 2839–2879at <https://ci.nii.ac.jp/naid/10011591188/en/>.

3. Conzelmann, E and Sandhoff, K. Partial enzyme deficiencies: residual activities and the development of neurological disorders. *Dev. Neurosci.* **6**: 58–71.

4. Kresse, H, Fuchs, W, Glössl, J, Holtfrerich, D and Gilberg, W (1981). Liberation of N-acetylglucosamine-6-sulfate by human beta-N-acetylhexosaminidase A. *J. Biol. Chem.* **256**: 12926–12932.

5. Mark, BL, Mahuran, DJ, Cherney, MM, Zhao, D, Knapp, S and James, MNG (2003). Crystal structure of human beta-hexosaminidase B: understanding the molecular basis of Sandhoff and Tay-Sachs disease. *J. Mol. Biol.* **327**: 1093–1109.

6. Lemieux, MJ, Mark, BL, Cherney, MM, Withers, SG, Mahuran, DJ and James, MNG (2006). Crystallographic structure of human beta-hexosaminidase A: interpretation of Tay-Sachs mutations and loss of GM2 ganglioside hydrolysis. *J. Mol. Biol.* **359**: 913–929.

7. Cachon-Gonzalez, MB, Zaccariotto, E and Cox, TM (2018). Genetics and Therapies for GM2 Gangliosidosis. *Curr. Gene Ther.* **18**: 68–89.

8. Dersh, D, Iwamoto, Y and Argon, Y (2016). Tay-Sachs disease mutations in HEXA target the α chain of hexosaminidase A to endoplasmic reticulum-associated degradation. *Mol. Biol. Cell* **27**: 3813–3827.

9. Kornfeld, S (1992). Structure and Function of the Mannose 6-Phosphate/Insulinlike Growth Factor II Receptors. *Annu. Rev. Biochem.* **61**: 307–330.

10. Mahuran, DJ (1998). The GM2 activator protein, its roles as a co-factor in GM2 hydrolysis and as a general glycolipid transport protein. *Biochim. Biophys. Acta (BBA)/Lipids Lipid Metab.* **1393**: 1–18.

11. Wendeler, M, Hoernschemeyer, J, Hoffmann, D, Kolter, T, Schwarzmann, G and Sandhoff, K (2004). Photoaffinity labelling of the Human GM2-activator protein. *Eur. J. Biochem.* **271**: 614–627.

12. Kaback, MM and Zeiger, RS (1972). Heterozygote Detection in Tay-Sachs Disease: A Prototype Community Screening Program for the Prevention of Recessive Genetic Disorders. In: Volk, BW and Aronson, SM (eds.). *Sphingolipids, Sphingolipidoses Allied Disord. Proc. Symp. Sphingolipidoses Allied Disord. held Brooklyn, New York, Oct. 25--27, 1971*, Springer US, Boston, MA: pp 613–632doi:10.1007/978-1-4757-6570-0_42.

13. Cecchi, AC, Vengoechea, ES, Kaseniit, KE, Hardy, MW, Kiger, LA, Mehta, N, *et al.* (2019). Screening for Tay-Sachs disease carriers by full-exon sequencing with novel variant interpretation outperforms enzyme testing in a pan-ethnic cohort. *Mol. Genet. Genomic Med.* **7**: e836.

14. Lawson, CA and Martin, DR (2016). Animal models of GM2 gangliosidosis: utility and limitations. In: Lawson, CA (ed.). *Appl. Clin. Genet.* **9**: 111–120.

15. Weitz, G and Proia, RL (1992). Analysis of the glycosylation and phosphorylation of the alpha-subunit of the lysosomal enzyme, beta-hexosaminidase A, by site-directed mutagenesis. *J. Biol. Chem.* **267**: 10039–10044.

16. Seyrantepe, V, Demir, SA, Timur, ZK, Von Gerichten, J, Marsching, C, Erdemli, E, *et al.* (2018). Murine Sialidase Neu3 facilitates GM2 degradation and bypass in mouse model of Tay-Sachs disease. *Exp. Neurol.* **299**: 26–41.

17. Leinekugel, P, Michel, S, Conzelmann, E and Sandhoff, K (1992). Quantitative correlation between the residual activity of beta-hexosaminidase A and arylsulfatase A and the severity of the resulting lysosomal storage disease. *Hum. Genet.* **88**: 513–523.

18. Navon, R and Proia, RL (1989). The mutations in Ashkenazi Jews with adult GM2 gangliosidosis, the adult form of Tay-Sachs disease. *Sci. (American Assoc. Adv. Sci.* **243**: 1471–1474.

19. Nakano, T, Muscillo, M, Ohno, K, Hoffman, AJ and Suzuki, K (1988). A Point Mutation in the Coding Sequence of the β-Hexosaminidase α Gene Results in Defective Processing of the Enzyme Protein in an Unusual GM2-Gangliosidosis Variant. *J. Neurochem.* **51**: 984–987.

20. Ohno, K, Saito, S, Sugawara, K and Sakuraba, H (2008). Structural consequences of amino acid substitutions causing Tay–Sachs disease. *Mol. Genet. Metab.* **94**: 462–468.

21. Brown, CA and Mahuran, DJ (1993). beta-Hexosaminidase isozymes from cells cotransfected with alpha and beta cDNA constructs: analysis of the alpha-subunit missense mutation associated with the adult form of Tay-Sachs disease. *Am. J. Hum. Genet.* **53**: 497–508.

22. Mueller, B, Klemm, EJ, Spooner, E, Claessen, JH and Ploegh, HL (2008). SEL1L nucleates a protein complex required for dislocation of misfolded glycoproteins. *Proc. Natl. Acad. Sci. U. S. A.* **105**: 12325–12330.

23. Mueller, B, Lilley, BN and Ploegh, HL (2006). SEL1L, the homologue of yeast Hrd3p, is involved in protein dislocation from the mammalian ER. *J. Cell Biol.* **175**: 261–270.

24. Tropak, MB, Reid, SP, Guiral, M, Withers, SG and Mahuran, D (2004). Pharmacological enhancement of beta-hexosaminidase activity in fibroblasts from adult Tay-Sachs and Sandhoff Patients. *J. Biol. Chem.* **279**: 13478–13487.

25. Tropak, MB and Mahuran, D (2007). Lending a helping hand, screening chemical libraries for compounds that enhance beta-hexosaminidase A activity in GM2 gangliosidosis cells. *FEBS J.* **274**: 4951–4961.

26. Maegawa, GHB, Tropak, M, Buttner, J, Stockley, T, Kok, F, Clarke, JTR, *et al.* (2007). Pyrimethamine as a potential pharmacological chaperone for late-onset forms of GM2 gangliosidosis. *J. Biol. Chem.* **282**: 9150–9161.

27. Clarke, JTR, Mahuran, DJ, Sathe, S, Kolodny, EH, Rigat, BA, Raiman, JA, *et al.* (2011). An open-label Phase I/II clinical trial of pyrimethamine for the treatment of patients affected with chronic GM2 gangliosidosis (Tay-Sachs or Sandhoff variants). *Mol. Genet. Metab.* **102**: 6–12.

28. Jim, RT and Elizaga, F V (1977). Development of chronic granulocytic leukemia in a patient treated with pyrimethamine. *Hawaii Med. J.* **36**: 173,176.

29. Rao Vunnam, R and Radin, NS (1980). Analogs of ceramide that inhibit glucocerebroside synthetase in mouse brain. *Chem. Phys. Lipids* **26**: 265–278.

30. Radin, NS (1996). Treatment of Gaucher disease with an enzyme inhibitor. *Glycoconj. J.* **13**: 153–157.

31. Butters, TD, Dwek, RA and Platt, FM (2005). Imino sugar inhibitors for treating the lysosomal glycosphingolipidoses. *Glycobiol.* **15**: 43R-52R.

32. Tallaksen, CME and Berg, JE (2009). Miglustat therapy in juvenile Sandhoff disease. *J. Inherit. Metab. Dis.* **32**: 289–293.

33. Wortmann, SB, Lefeber, DJ, Dekomien, G, Willemsen, MAAP, Wevers, RA and Morava, E (2009). Substrate deprivation therapy in juvenile Sandhoff disease. *J. Inherit. Metab. Dis.* **32**: 307–311.

34. Shapiro, BE, Pastores, GM, Gianutsos, J, Luzy, C and Kolodny, EH (2009). Miglustat in late-onset Tay-Sachs disease: a 12-month, randomized, controlled clinical study with 24 months of extended treatment. *Genet. Med.* **11**: 425–433.

35. Matsuoka, K, Tamura, T, Tsuji, D, Dohzono, Y, Kitakaze, K, Ohno, K, *et al.* (2011). Therapeutic potential of intracerebroventricular replacement of modified human β-hexosaminidase B for GM2 gangliosidosis. *Mol. Ther.* **19**: 1017–1024.

36. Sinici, I, Yonekawa, S, Tkachyova, I, Gray, SJ, Samulski, RJ, Wakarchuk, W, *et al.* (2013). In cellulo examination of a beta-alpha hybrid construct of beta-hexosaminidase A subunits, reported to interact with the GM2 activator protein and hydrolyze GM2 ganglioside. *PLoS One* **8**: e57908.

37. Kitakaze, K, Mizutani, Y, Sugiyama, E, Tasaki, C, Tsuji, D, Maita, N, *et al.* (2016). Protease-resistant modified human β-hexosaminidase B ameliorates symptoms in GM2 gangliosidosis model. *J. Clin. Invest.* **126**: 1691–1703.

38. Alam, MI, Beg, S, Samad, A, Baboota, S, Kohli, K, Ali, J, *et al.* (2010). Strategy for

effective brain drug delivery. *Eur. J. Pharm. Sci.* **40**: 385–403.

39. Cohen-Pfeffer, JL, Gururangan, S, Lester, T, Lim, DA, Shaywitz, AJ, Westphal, M, *et al.* (2017). Intracerebroventricular Delivery as a Safe, Long-Term Route of Drug Administration. *Pediatr. Neurol.* **67**: 23–35.

40. Stroobants, S, Gerlach, D, Matthes, F, Hartmann, D, Fogh, J, Gieselmann, V, *et al.* (2011). Intracerebroventricular enzyme infusion corrects central nervous system pathology and dysfunction in a mouse model of metachromatic leukodystrophy. *Hum. Mol. Genet.* **20**: 2760–2769.

41. Liu, L, Lee, W-S, Doray, B and Kornfeld, S (2017). Engineering of GlcNAc-1-Phosphotransferase for Production of Highly Phosphorylated Lysosomal Enzymes for Enzyme Replacement Therapy. *Mol. Ther. - Methods Clin. Dev.* **5**: 59–65.

42. Tropak, MB, Yonekawa, S, Karumuthil-Melethil, S, Thompson, P, Wakarchuk, W, Gray, SJ, *et al.* (2016). Construction of a hybrid β-hexosaminidase subunit capable of forming stable homodimers that hydrolyze GM2 ganglioside in vivo. *Mol. Ther. - Methods Clin. Dev.* **3**: 15057.

43. Gray, SJ (2013). Gene therapy and neurodevelopmental disorders. *Neuropharmacology* **68**: 136–142.

44. Karumuthil-Melethil, S, Nagabhushan Kalburgi, S, Thompson, P, Tropak, M, Kaytor, MD, Keimel, JG, *et al.* (2016). Novel Vector Design and Hexosaminidase Variant Enabling Self-Complementary Adeno-Associated Virus for the Treatment of Tay-Sachs Disease. *Hum. Gene Ther.* **27**: 509–521.

45. Pulicherla, N, Shen, S, Yadav, S, Debbink, K, Govindasamy, L, Agbandje-McKenna, M, *et al.* (2011). Engineering liver-detargeted AAV9 vectors for cardiac and musculoskeletal gene transfer. *Mol. Ther.* **19**: 1070–1078.

46. Osmon, KJL, Woodley, E, Thompson, P, Ong, K, Karumuthil-Melethil, S, Keimel, JG, *et al.* (2016). Systemic Gene Transfer of a Hexosaminidase Variant Using an scAAV9.47 Vector Corrects GM2 Gangliosidosis in Sandhoff Mice. *Hum. Gene Ther.* **27**: 497–508.

47. Li, Z, Michael, IP, Zhou, D, Nagy, A and Rini, JM (2013). Simple piggyBac transposon-based mammalian cell expression system for inducible protein production. *Proc. Natl. Acad. Sci. U. S. A.* **110**: 5004–5009.

48. Liu, L, Lee, W-S, Doray, B and Kornfeld, S (2017). Engineering of GlcNAc-1-Phosphotransferase for Production of Highly Phosphorylated Lysosomal Enzymes for Enzyme Replacement Therapy. *Mol. Ther. - Methods Clin. Dev.* **5**: 59–65.

49. Meyerson, M, Counter, CM, Eaton, EN, Ellisen, LW, Steiner, P, Caddle, SD, *et al.* (1997). hEST2, the putative human telomerase catalytic subunit gene, is up-regulated in tumor cells and during immortalization. *Cell* **90**: 785–795.

50. McIlvaine, TC. A buffer solution for colorimetric comparison. *J. Biol. Chem.*at <http://worldveg.tind.io/record/17952>.

51. Longo, PA, Kavran, JM, Kim, M-S and Leahy, DJ (2013). Transient mammalian cell transfection with polyethylenimine (PEI). *Methods Enzymol.* **529**: 227–240.

52. Golding, CG, Lamboo, LL, Beniac, DR and Booth, TF (2016). The scanning electron microscope in microbiology and diagnosis of infectious disease. *Sci Rep* **6**: 26516.

53. Kabsch, W (2010). XDS. *Acta Crystallogr. Sect. D* **66**: 125–132.

54. Emsley, P, Lohkamp, B, Scott, WG and Cowtan, K (2010). Features and development of {\it Coot}. *Acta Crystallogr. Sect. D* **66**: 486–501.

55. Afonine, P V, Grosse-Kunstleve, RW, Echols, N, Headd, JJ, Moriarty, NW, Mustyakimov, M, *et al.* (2012). Towards automated crystallographic structure refinement with {\it phenix.refine}. *Acta Crystallogr. Sect. D* **68**: 352–367.

56. Anheuser, S, Breiden, B, Schwarzmann, G and Sandhoff, K (2015). Membrane lipids regulate ganglioside GM2 catabolism and GM2 activator protein activity. *J. Lipid Res.* **56**: 1747–1761.

57. Inui, K and Wenger, DA (1984). Usefulness of 4-methylumbelliferyl-6- sulfo-2-acetamido-2-deoxy-β-D-glucopyranoside for the diagnosis of GM2 gangliosidoses in leukocytes. *Clin. Genet.* **26**: 318–321.

58. Hou, Y, Tse, R and Mahuran, DJ (1996). Direct Determination of the Substrate Specificity of the α-Active Site in Heterodimeric β-Hexosaminidase A. *Biochemistry* **35**: 3963–3969.

59. Tsuji, D, Akeboshi, H, Matsuoka, K, Yasuoka, H, Miyasaki, E, Kasahara, Y, *et al.* Highly phosphomannosylated enzyme replacement therapy for GM2 gangliosidosis. *Ann. Neurol.* **69**: 691,701.

60. Hawkes, C and Kar, S (2003). Insulin-like growth factor-II/mannose-6-phosphate receptor: widespread distribution in neurons of the central nervous system including those expressing cholinergic phenotype. *J. Comp. Neurol.* **458**: 113–127.

61. Wu, Y-P, Proia, RL and Neufeld, EF (2004). Deletion of Macrophage-Inflammatory

Protein 1α Retards Neurodegeneration in Sandhoff Disease Mice. *Proc. Natl. Acad. Sci. U. S. A.* **101**: 8425–8430.

62. Schrödinger, LLC (2015). *The {PyMOL} Molecular Graphics System, Version~1.8*.

63. Sandhoff, K and Harzer, K (2013). Gangliosides and gangliosidoses: Principles of molecular and metabolic pathogenesis. *J. Neurosci.* **33**: 10195–10208.

64. Pettersen, EF, Goddard, TD, Huang, CC, Couch, GS, Greenblatt, DM, Meng, EC, *et al.* (2004). UCSF Chimera—A visualization system for exploratory research and analysis. *J. Comput. Chem.* **25**: 1605–1612.

65. Hill, CH, Cook, G, Spratley, SJ, Fawke, S, Graham, SC and Deane, JE (2018). The mechanism of glycosphingolipid degradation revealed by a GALC-SapA complex structuredoi:10.17863/CAM.18694.

66. Woodley, E, Osmon, KJL, Thompson, P, Richmond, C, Chen, Z, Gray, SJ, *et al.* (2018). Efficacy of a Bicistronic Vector for Correction of Sandhoff Disease in a Mouse Model. *Mol. Ther. Methods Clin. Dev.* **12**: 47–57.

67. Ou, L, Przybilla, MJ, Tăbăran, A-F, Overn, P, O'Sullivan, MG, Jiang, X, *et al.* (2020). A novel gene editing system to treat both Tay–Sachs and Sandhoff diseases. *Gene Ther.*doi:10.1038/s41434-019-0120-5.

Chapter 5: Supplementary Figures

GTAAGCCTATCCCTAACCCTCTCCTCGGTCTCGATTCTACGCGTACCGGTCATCATCA
CCATCACCATTGAGTTT

GB.2.201.1 T7 Forward

GTAAGCCTATCCCTAACCCTCTCCTCGGTCTCGATTCTACGCGTACCGGTTGAGTTT

GB.2.201.2 BGH Reverse

GTAAGCCTATCCCTAACCCTCTCCTCGGTCTCGATTCTACGCGTACCGGTTGAGTTT

Supplementary Figure 1: Sequence alignment of GlcNAc-1-PT-NoHis. The T7 forward primer and BGH reverse primer used was provided by TCAG (SickKids, Ontario). The His tag deletion is highlighted in purple.

GGGACTGCT**GCTGGACACTA**GCCGCCATTATCTTCCGC**TTAAG**TCCATTCTGGATA
CCCTCGACGTGATGGCATACAACAAACTCAATGTGTTCCACTGGCATCTGGTGGACG
ACCAGTCATTTCCCTACGAGTCCTTCACCTTCCCCGAACTCATGAGGAAGGGAAGCT
ACTCTCTCAGCCACATCTACACCGCCCAAGACGTCAAGGAAGTCATCGAATATGCAC
GCCTGCGCGGAATTAGAGTGCTCGCCGAGTTCGACACCCCTGGGCACACCCTGAGCT
GGGGACCTGGCATCCCTGGTCTGCTCACTCCCTGCTATTCAGGGTCAGAACCTTCCG
GTACTTTTGGCCCTGTCAATCCTAGCCTGAACAATACTTACGAGTTTATGTCTACTTT
CTTCCTTGAAGTCTCATCAGTCTTTCCAGACTTCTATCTGCATCTCGGAGGTGAT**GAA**
GTGGACTTCACCTGTTGGAAGTCAAACCCCGAAATTCAAGACTTTATGCGGAAGAA
GGGTTTCGGAGAGGATTTCAAACAACTGGAGAGCTTCTACATCCAGACCCTTCTCGA
CATCGTGTCCTCATACGGGAAAGGTTACGTGGTCTGGCAGGAAGTGTTCGACAATAA
GGTGAAGATTCAGCCCGACACCATTATCCAAGTCTGGCGGGAGGACATCCCAGTGA
ACTACATGAAGGAACTTGAGCTGGTGACTAAGGCTGGGTTCCGCGCTCTTCTC**AGC**G
CTCCATGGTATCTCAATCGGATCTCTTACGGACAGGATTGGAGGAAGTTCTAC**AAAG**
TCGAACCCCTGGCTTT

Supplementary Figure 2: Sequence for gBlock. The sequence of the synthetic double-stranded DNA fragment (891bp) containing a single amino acid mutation (in purple). The nucleotide sequence selected for primers is shown in green. The cut sites of AflII (TTAAG) and AfeI (AGC) are shown in red.

HexM Nucleotide Sequence
GAT**GAA**GTGGACTTCACCTGTTGGAAGTCAAACCCCGAAATTCAAGACTTTATGCGG
AAG

GB2.31.07-user_added.ab1 (reversed)
GAT**CAG**GTGGACTTCACCTGTTGGAAGTCAAACCCCGAAATTCAAGACTTTATGCGG
AAG

GB2.31.08-user_added.ab1
GAT**CAG**GTGGACTTCACCTGTTGGAAGTCAAACCCCGAAATTCAAGACTTTATGCGG
AAG

Supplementary Figure 3: Sequence alignment of HexME322Q. The primers used were previously described to amplify the gBlock. The single amino acid substitution is shown in purple. Sequencing was conducted by The Center for Applied Genomics (TCAG) (SickKids, Ontario)